

**Metal free room temperature phosphorescence from
molecular self-interaction in the solid state**

Journal:	<i>Journal of Materials Chemistry C</i>
Manuscript ID	Draft
Article Type:	Review Article
Date Submitted by the Author:	n/a
Complete List of Authors:	Cariati, Elena; Universit� degli Studi di Milano, Forni, Alessandra; ISTM-CNR, Universita` di Milano, Via Venezian 21, I- 20133 Milan, Italy, Lucenti, Elena; ISTM-CNR, Botta, Chiara; CNR, ISMAC



UNIVERSITÀ DEGLI STUDI DI MILANO

DIPARTIMENTO DI CHIMICA

Via Golgi 19 - 20133 Milano (ITALY)

Milano, February 28 2018

To the Editor of *Journal of Materials Chemistry C*,

Dear Editor,

we submit to your kind attention the invited Review entitled:

“Metal free room temperature phosphorescence from molecular self-interaction in the solid state”

by Alessandra Forni, Elena Lucenti, Chiara Botta, and myself, for publication in *J. Mater. Chem. C*.

Organic room-temperature-phosphorescent (RTP) materials are very attractive owing to their potential value in organic light-emitting diodes (OLEDs), optical storage, bioimaging, sensors, security, and many other applications. They are also very good candidates for replacing phosphorescent complexes containing expensive metals. In this context, great effort has been made in the development of solid organic RTP materials, and several strategies have been proposed leading to significant progresses. However, the properties of organic solids in the triplet excited state are affected by many factors and, therefore, it remains a great challenge to design/prepare highly efficient organic RTP solids. Pioneering research carried out by Tang and co-workers demonstrated that intermolecular interactions could not only suppress ACQ (aggregation caused quenching behavior) (*Chem. Commun.*, **2001**, 1740) but also stabilize the triplet excitons and consequently trigger RTP (*J. Phys. Chem. C*, **2010**, *114*, 6090). In addition, very recently, An and co-workers reported ultra-long phosphorescent emission features in structures of planar organic molecules coupled in H-aggregates (*Nat. Mater.*, **2015**, *14*, 685). The stabilized excited state, which functions as an energy trap at a lower energy level, may delocalize on several neighboring molecules, offering suppressed radiative and non-radiative deactivation decay rates in favour of long-lived excited states and ultralong phosphorescence. Similarly, we have reported on a new family of organic materials (namely cyclic-triimidazole and its halogenated derivatives) displaying RTP due to H-

Prof. Elena Cariati

Tel: +39.0250314370 Fax: +39.0250314405 e-mail: elena.cariati@unimi.it



UNIVERSITÀ DEGLI STUDI DI MILANO

DIPARTIMENTO DI CHIMICA

Via Golgi 19 - 20133 Milano (ITALY)

aggregation and halogen-bonding (*J. Phys. Chem. Lett.*, **2017**, *8*, 1894 and *Angew. Chem. Int. Ed.*, **2017**, *56*, 16302).

Recently, numerous reviews have been published on organic RTP solid materials in which phosphorescence is switched on either by rigidification in crystals or polymeric matrix and/or by interchromophoric interaction with other molecules of the same type or a different type. In the present review we focus on organic molecules whose solid state RTP is switched on by intermolecular interaction among one-type only molecules. We have identified essentially two kinds of intermolecular self-interactions which are able to switch on RTP, namely halogen bonding (XB) and π - π interactions. After recalling a few basic concepts underlying emission phenomena, we present a selection of examples where XB and π - π interactions are involved, separately or in conjunction, in switching on interaction-induced RTP. Due to difficulty in interpreting the mechanism at the basis of the photophysical behavior of the material, in some cases different suggestions have been formulated for the same luminogen by different authors. In such cases, we have collected and critically reviewed the different works referring to the same material or class of compounds even though mechanisms other than XB and π - π interactions are suggested. We believe that this Review would be of great interest for the readers of *J. Mater. Chem. C* being helpful in the understanding of a field of wide and increasing importance.

Best regards,

Elena Cariati



Journal Name

ARTICLE

Metal free room temperature phosphorescence from molecular self-interaction in the solid state

Received 00th January 20xx,
Accepted 00th January 20xx

DOI: 10.1039/x0xx00000x

www.rsc.org/

Alessandra Forni,^a Elena Lucenti,^a Chiara Botta^b and Elena Cariati^{*c}

Purely organic materials showing solid state room temperature phosphorescence (RTP) are receiving an ever growing interest due to their low toxicity, cost and environmental load with respect to their organometallic counterparts. In addition, specific features potentially associated with organic phosphorescent materials, such as long afterglow lifetimes, have opened the way to new possible applications including low-cost anti-counterfeiting technologies, temperature monitoring, sensing and bio-imaging. RTP of organic molecules is here reviewed for the cases where intermolecular interactions among one-type only molecules are involved. In particular, the selection is focused on papers regarding self-interactions of halogen bonding (XB) and π - π type. After recalling a few basic concepts underlying emission phenomena, a selection of examples where XB and π - π interactions are involved, separately or in conjunction, is reported. In the cases where different interpretations have been given for the same class of molecules, we have gathered and discussed the different suggested mechanisms.

Introduction

Room temperature phosphorescence (RTP) has been for years the realm of metal containing compounds.¹ This can be understood based on the requirement of strong spin-orbit coupling (SOC) to produce efficient intersystem crossing (ISC) and to the long lifetime of the phosphorescent excited state of organic molecules which is prone to be quenched by dioxygen and molecular motions. However, already in 1978 Bilen et al.² reported for pure crystalline solids of some organic compounds (including carbazole, dibenzothiophene, dibenzofuran and triphenylene) an unusual RT afterglow emission. Since this early report, purely organic materials showing RTP have received an ever growing interest because they offer many advantages with respect to their organometallic counterparts. In particular, organic materials are characterized by a low toxicity, cost and environmental load, as a consequence of the removal of toxic and generally very expensive metals (i.e. Ru(II), Os(II), Ir(III), Rh(III), Pt(II)), largely used for optoelectronic and biological applications. Moreover, specific features potentially associated with organic phosphorescent materials, such as long afterglow lifetimes, have opened the way to new possible applications

including low-cost anti-counterfeiting technologies, temperature monitoring, sensing and bio-imaging.³

At the same time, it has been recognized that RTP from organic compounds is actually a more frequent phenomenon than commonly believed. This is particularly true for solids and in fact fundamental for this new impetus have been the pioneering works of Luo et al.⁴ and An et al.⁵ on aggregation induced emission (AIE) which have allowed to disclose the extent of the phenomenon. In the AIE process, molecules which are not emissive or weakly so in dilute solutions are induced to emit efficiently by aggregate formation. AIE is the opposite of the more frequently observed phenomenon of aggregation-caused quenching (ACQ) which for a long time has hampered the development of efficient solid-state luminophores. The origin of AIE was found mainly in the restriction of molecular motions such as rotations (RIR) and vibrations which, in solution, are responsible for energy dissipation, i.e., nonradiative decay from excited states.⁴⁻⁶ In the aggregate (crystalline or amorphous) phase, intramolecular motions are locked by the rigid environment, allowing the luminogens to radiatively decay and become even strong fluorescent and/or phosphorescent emitters, as demonstrated by time resolved and ultrafast pump-probe spectroscopy, and supported by Time Dependent Density Functional Theory (TDDFT) calculations.⁷⁻⁹ Particularly intriguing are materials showing crystallization induced emission (CIE), i.e. materials where intramolecular motions are still active in the amorphous state while are suppressed in the crystal by specific intermolecular interactions, typically C-H \cdots π , C-H \cdots O, C-H \cdots X (X=halogen atom) and N-H \cdots O hydrogen bonds, besides

^a *ISTM-CNR, INSTM RU via Golgi 19, 20133 Milano (Italy).*

^b *ISMAL-CNR, INSTM RU Via Corti 12, 20133 Milano (Italy).*

^c *Department of Chemistry Università degli Studi di Milano and INSTM RU via Golgi 19, 20133 Milano (Italy). E-mail: elena.cariati@unimi.it.*

isotropic crystal packing forces.¹⁰⁻¹² While organic CIE compounds are generally characterized by prompt fluorescence, only few examples of crystallization induced phosphorescence (CIP) from organic materials have been reported since the early report by Bilen et al.² and the pioneering systematic investigations by Tang and coworkers.¹³ In these CIP materials, the most evident role of crystal packing is that of suppressing molecular motions (vibrations and conformational rearrangements) so as to minimize the non-radiative deactivation processes of triplet excitons. In addition, densely packed structures can protect from oxygen quenching. However, rigidification and suppression of quenching do not represent the only role played by the crystal structure in turning on RTP. Specific intermolecular interaction can, in fact, be decisive on this regard as testified by the increasing number of publications underlying this aspect. Very intriguing are molecules with similar chemical structures but different packing modes and RTP properties which allow to gain more insight into the crystal structure-emissive properties relationship.

In some cases, organic RTP may persist for a long time (lifetimes longer than 100 ms and approaching 1 s and more) after cessation of excitation (afterglow emission), a feature which is found in inorganic phosphors¹⁴ but it is extremely rare in organometallic RTP compounds¹⁵ owing to the small lifetimes of their triplet excitons. Such room temperature ultralong phosphorescence (RTUP) has been recognized to occur in special cases, for example when the molecular organization in a particular crystal structure (e.g. H aggregates) is able to provide a stabilization of the excited triplet state by trapping triplet excitons and extending both their radiative and non-radiative lifetimes. Recently, numerous reviews have been reported on organic RTP solid materials in which phosphorescence is switched on either by rigidification in crystals or polymeric matrix and/or by interchromophoric interaction with other molecules of the same type or a different type.^{3,16-23} The latter case shows up for example in two-component co-crystals where one of the two molecules contains a halogen atom which plays the role of the heavy atom.^{24,25}

Here we focus on organic molecules whose solid state RTP is switched on by intermolecular interactions among one-type only molecules. We have identified essentially two kinds of intermolecular self-interactions which are able to switch on RTP, namely halogen bonding (XB) and π - π interactions, though other mechanisms, as discussed below, have been proposed to explain in particular RTUP emission for some crystals. The difficult task here is to discriminate between these cases and those in which such interactions act in the same way as many others typically found in organic solids, whose role in RTP is mainly to restrict molecular motions. A strong but not sufficient indication would be a different phosphorescent behavior of the aggregated phase at RT with respect to that of the isolated molecule in rigidified solution or matrix. Isolated molecules could be not phosphorescent at all or with a shifted phosphorescent emission. Even in the latter case, however, the discrimination is not easy: the shifted phosphorescence of the aggregated phase could be originated by a different molecular

conformation induced by the crystal packing with respect to that of the isolated molecule.²⁶⁻²⁸

In the present review, after recalling a few basic concepts underlying emission phenomena, we present a selection of examples where XB and π - π interactions are involved, separately or in conjunction, in switching on interaction-induced RTP. Due to difficulty in interpreting the mechanism at the basis of the photophysical behavior of the material, in some cases different suggestions have been formulated for the same luminogen by different authors. In such cases, we have collected the different works referring to the same material or class of compounds even though mechanisms other than XB and π - π interactions are suggested.

Description of emission phenomena

As schematically shown in Figure 1, when an organic chromophore absorbs one photon of proper energy, one electron is promoted from the ground singlet (S_0) state to a high energy singlet (S_n) state and generally relaxes through non-radiative internal conversion (IC) to the lowest excited singlet state (S_1). Fluorescence is the result of the fast (lifetimes, τ , typically in the ns range) radiative deactivation (rate constant k_F) from S_1 to S_0 . The singlet excited state can also relax non-radiatively, either to the ground state through IC (rate constant k_{NR}^F) or to a triplet state (rate constant k_{ST}) through ISC when SOC is high since singlet-triplet transitions are forbidden by the spin selection rule. In purely organic systems, SOC is generally very low and therefore S-T ISC processes are not efficient ($k_{ST} \sim 10^7$ - 10^8 sec⁻¹). However they can be facilitated by the presence of carbonyls, heteroatoms or heavy halogens, by small energy gaps (ΔE_{ST}) between the involved singlet and triplet states and by large overlap between their vibrational functions.^{29,30} In organic aromatic molecules with large π -conjugation frameworks, ISC is weak because their lowest-lying levels have large ΔE_{ST} while compounds with n - π^* type transitions, like benzophenone (Bp), have smaller exchange integrals and consequently small ΔE_{ST} values, which facilitate ISC processes. Moreover, according to El-Sayed's rule,³¹ the ISC rate constant k_{ST} depends on the nature of the two states involved in the electronic transitions, and in particular it is larger when the two states are of different orbital parentage ($^1n\pi^* \rightarrow ^3\pi\pi^*$ or $^1\pi\pi^* \rightarrow ^3n\pi^*$).

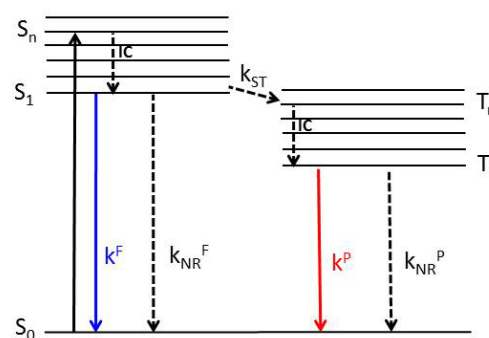


Figure 1. Schematic representation of the main absorption and emission processes of an organic molecule.

After population of an excited T_n triplet state and its IC relaxation to T_1 , the radiative recombination from T_1 to S_0 gives rise to phosphorescence (rate constant k_P). This process is

slower (typically in the 10 μ s-100ms range) with respect to fluorescence due to the forbidden nature of T-S transitions. In addition, phosphorescence is in competition with non-radiative intramolecular deactivation to S₀ (rate constant k_{NR}^P) through ISC and molecular motions (rotations and/or vibrations), and through interactions with quenchers (oxygen and humidity) whose probability is increased by the long lifetime nature of the triplet states. In general, due to the competitive non-radiative deactivation processes, phosphorescence from pure organic molecules is observed only in the absence of oxygen and by blocking molecular motions. This is usually obtained by lowering the temperature or by embedding the chromophores into a rigid matrix at RT.^{32,33}

When the T₁ triplet state of an organic molecule is of ³(n, π^*) character, the rate constants of the transition to the ground state are larger than expected from triplet states of ³(π,π^*) type (El-Sayed's rule), therefore the molecule might exhibit efficient short-lived phosphorescence (10 μ s-100ms). Differently, when the T₁ state is of ³(π,π^*) character, phosphorescence lifetimes become longer but the emission is more prone to quenching phenomena. However, as it will be shown by the many examples reported in this review, proper intermolecular interactions in purely organic crystals may stabilize the triplet state resulting in RTUP (lifetimes in the 100ms-10s range) even under ambient conditions. The persistent luminescence of organic afterglow materials is therefore the result of the slow radiative decay of stabilized long-lived triplet excited states for which $k^P > k_{NR}^P$.

Halogen bonding induced RTP

It is well known that the presence of halogen atoms, such as bromine and iodine, on an organic molecule enhances SOC due to their heavy atom effect favoring S-T ISC. This results in the quenching of fluorescence on one side and, on the other, either in the possible enhancement of phosphorescence or in non radiative (T-S ISC) relaxation to the ground state in a not predictable way.

When going to the solid state, intermolecular interactions involving halogen atoms may positively contribute to the observed photophysical behavior. An early example of the effect of the halogen atom on organic phosphorescence is provided by halogenated Bp derivatives.¹³ With a lone pair of electrons on the oxygen atom, the aromatic carbonyl favors SOC, which allows for the intrinsic triplet generation through ISC. However, Bp and its derivatives are not luminescent in solution at RT but highly phosphorescent at 77K and in the solid state. Thus phosphorescence is interpreted as due to conformational rigidification. In the crystal phase the presence of halogen atoms contributes to rigidify the molecular conformation through halogen bonding (XB) resulting in crystallization induced phosphorescent (CIP) materials.

In the same way, several studies regarding solid state RTP of halogenated organic molecules have appeared in the literature where phosphorescence is ascribed to rigidification together with intrinsic heavy atom effect. However, besides rigidification, the presence of the halogen atom may induce

intermolecular electronic coupling (IEC) prone to alter the photophysical behavior of the isolated chromophore. This is the case of co-crystals in which XB is exploited to produce phosphorescence through an extrinsic heavy atom effect.²⁵ Limiting to the cases of single component crystals, the boundary between rigidification and IEC is very subtle and the number of reports in which IEC associated with XB is explicitly mentioned is strongly reduced. A way to support the presence of IEC would be the photophysical characterization of the luminophore in solution at low temperature: if the phosphorescence is turned on or intensified, molecular rigidification alone is at the basis of the observed solid state RTP. Unfortunately, the low temperature molecular characterization is often lacking in the reported studies.

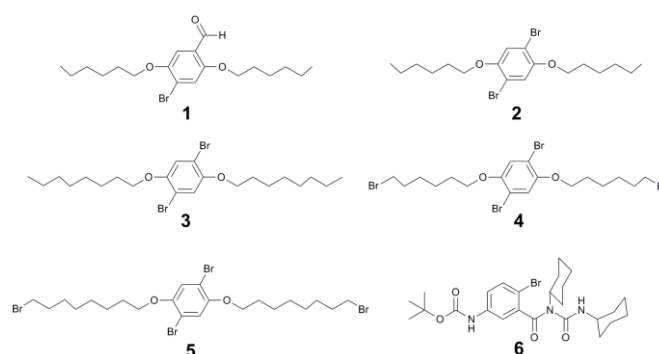


Chart 1. Compounds with XB induced RT

We have identified the following studies as proper examples of XB IEC self-induced RTP. The first report is by Bolton et al.³⁴ on 2,5-dihexyloxy-4-bromobenzaldehyde (**1**). When excited at 360 nm in chloroform, the chromophore is weakly fluorescent (420 nm, photoluminescence quantum yield, Φ , equal to 0.5% and $\tau = 0.5$ ns) but becomes also phosphorescent (500 nm, $\Phi_p = 2.9\%$ and $\tau = 5.4$ ms) in its crystal form. Single-crystal X-ray diffraction analysis (XRD) revealed the presence of an extremely close contact between the carbonyl oxygen and the bromine of the neighboring molecule ($r_{Br...O} = 2.86$ Å, see Figure 2). Based on this and supported by the observation that phosphorescence was activated in real time as crystals grew from the molten liquid phase, the authors suggested that the observed C-Br...O=C XB is responsible for the green phosphorescence of the compound. In agreement, the ratio of phosphorescence to fluorescence was correlated to the quality of the crystals: those quickly grown from drop-casting predominantly exhibited fluorescence, while phosphorescence dominated the spectrum of those more slowly formed. According to the authors, the close contact between the bromine and the carbonyl oxygen allows to promote SOC where the triplet is produced, i.e. the carbonyl unit, thus facilitating ISC.

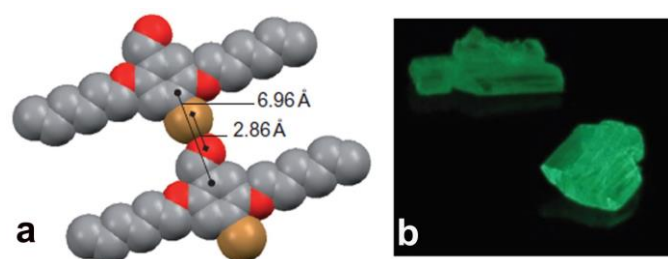


Figure 2. a) Crystal packing of **1**, highlighting the carbonyl oxygen–bromine distance defining the XB; b) Photograph of crystals of **1** under 365 nm UV light. (Adapted with permission from ref. 34. Copyright 2011, Springer Nature).

Later on, Shi et al.³⁵ demonstrated that Br⋯Br XBs are effective in inducing RTP as observed in crystal structures of a series of similar dibromobenzene derivatives. In particular, multiple Br⋯Br interactions are associated with higher luminescence efficiency with respect to analogue structures with single Br⋯Br XB. The authors investigated four compounds, namely, 1,4-dibromo-2,5-bis(hexyloxy)benzene (**2**), 1,4-dibromo-2,5-bis(octyloxy)benzene (**3**), 1,4-dibromo-2,5-bis((6-bromohexyl)oxy)benzene (**4**) and 1,4-dibromo-2,5-bis((8-bromooctyl)oxy)-benzene (**5**), the two latter bearing additional bromine functionalization at the end of the alkylic units. The four luminophores are not emissive in solution but quite so in the solid state. In particular, the di-brominated compounds possess intense green emissions ($\lambda_{em} = 500$ nm, phosphorescence quantum yield, Φ_p , equal to 3.4 and 8.9% for **2** and **3**, respectively, τ in the millisecond regime) and weak blue fluorescence ($\lambda_{em} \approx 380$ nm, τ in the nanosecond scale), while tetra-brominated ones display only strong green phosphorescence ($\Phi_p = 21.9$ and 13.1% for **4** and **5**, respectively, τ in the millisecond regime). Analysis of crystal structures revealed that all of these organic phosphors are arranged in layers with a distance of around 3.7 Å between neighboring layers. Within a layer, all luminogens are locked by various intermolecular forces including C–Br⋯Br–C and C–H⋯Br interactions (see Figure 3). In both di-brominated compounds, there are only single Br⋯Br interactions with distances of 3.405 (**2**) and 3.380 Å (**3**), respectively. On the other side, triple Br⋯Br halogen bonds (3.575, 4.157 and 4.241 Å) were observed in **4**, while double Br⋯Br interactions (3.577 and 4.244 Å) in **5**. The authors correlated the different phosphorescence efficiencies to such different XB pattern. In particular, the improved phosphorescence quantum yields of both **4** and **5** solids was ascribed to the synergistic effects of the promotion of Br–cluster interaction and the suppression of triplet–triplet annihilation between adjacent molecules.

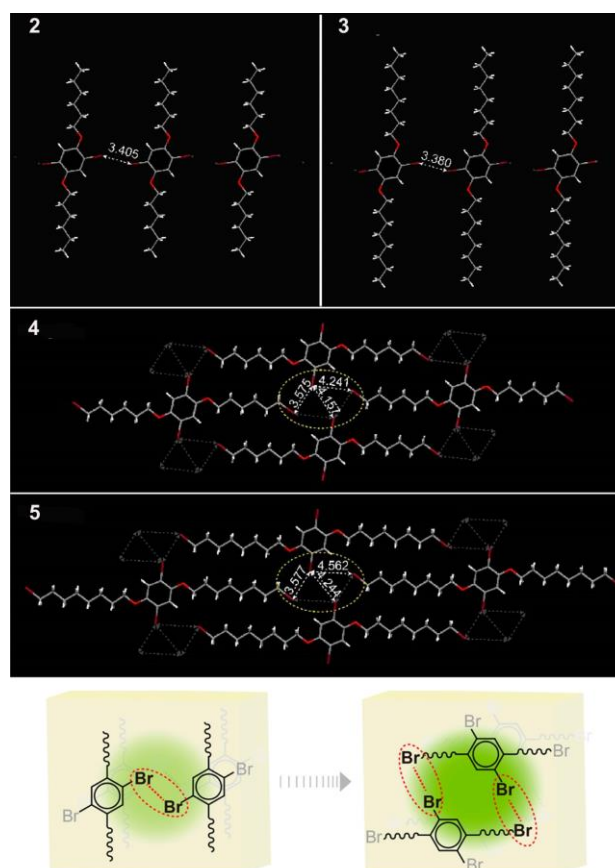


Figure 3. Top: Perspective views of the XB in single crystals of dibromobenzene derivatives **2**, **3**, **4** and **5**. Bottom: Schematic presentation of heavy-atom interactions able to enhance organic phosphorescence. (Adapted with permission from ref. 35. Copyright 2016, American Chemical Society).

Maity et al.³⁶ demonstrated a correlation between XB strength and increase in RTP lifetime and intensity. They observed different RTP efficiencies for a brominated Boc and N,N'-dicyclohexylurea capped γ -amino acid, **6**, in the solid state as a result of crystallization in different polar aprotic (ethyl acetate) and polar protic (methanol) solvents. While the chloroform solution of the material shows weak blue fluorescence ($\lambda_{em} = 380$ nm, τ in the nanosecond regime), the crystal phase is characterized by the presence of a green phosphorescence ($\lambda_{em} = 467, 482$ and 492 nm) together with fluorescence. The relative intensity of the two components varies with crystallization solvent. In particular, phosphorescence dominates the spectrum of the compound crystallized from methanol. A similar trend was determined for phosphorescence lifetimes, being longer for the methanol crystallized sample (13 μ s) than that of the ethyl acetate one (11 μ s). Since the emission spectrum in glassy solutions (77 K) exhibits fluorescence with no additional peak in the range 460–500 nm, the RTP observed in the crystal phase was associated with the synergistic effect of crystalline rigidification and C–Br⋯O=C XB, whose strength increases from ethyl acetate (3.29 Å) to methanol (3.15 Å, Figure 4a and b). In both solvents, the compound crystallizes in the same crystalline form without cocrystallized solvent

molecules with only minor differences in cell parameters. Thus, the quite different XB length could be ascribed to different molecular conformations (Figure 4a and b), which leads as well to two different macroscopic morphologies, nanofibrillar from ethyl acetate and spherical from methanol solution (Figure 4c and d).

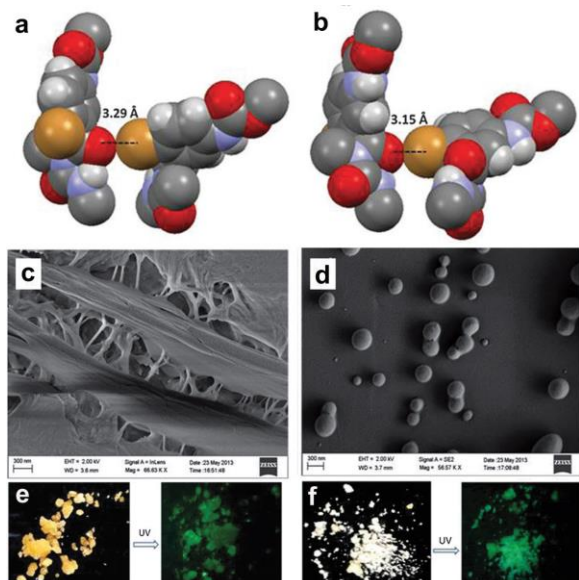


Figure 4. Top: The C=O...Br-C XB in crystal of **6** from (a) ethyl acetate and (b) methanol solution. Middle: field emission scanning electron microscopy images of **6** obtained from (c) ethyl acetate and (d) methanol solution. Bottom: the photographs of the crystals obtained from (e) ethyl acetate and (f) methanol solution under laboratory light and 254 nm UV light. (Adapted from ref. 36 with permission from The Royal Society of Chemistry).



Journal Name

ARTICLE

Table 1 RTP Emission Maxima (λ_{em}), Phosphorescence Quantum Efficiency (Φ_p), and Lifetimes (τ) of compounds 1-6

Label	Compound Structure	Phosphorescence			Reference
		λ_{em} (nm)	Φ_p (%)	τ (ms)	
1		500	2.9	5.4	34
2		515	3.4	8.3	35
3		492	8.9	6.7	35
4		507	21.9	6.5	35
5		502, 535	13.1	6.4 ^a	35
6		467, 482, 492	n.d.	11 μ s ^b 13 μ s ^c	36

^a Measured at 502nm; ^b Crystals obtained from AcOEt; ^c Crystals obtained from MeOH

π - π interaction induced RTP

Despite the common belief that strong intermolecular π - π stacking interactions in aggregates result in quenching of the molecular emission,^{37,38} it has been shown that in some cases they are beneficial for RTP and RTUP emissions. In 1958, McRae and Kasha reported a paper³⁹ where the concept of phosphorescence enhancement upon aggregation of dye molecules was highlighted. According to the authors' simplified model, when aggregation of N molecules occurs, the upper energy states of each monomer 0-0 transition spread into an N -fold band of levels (exciton band). Since exciton splitting depends on the oscillator strength of the transition, only the singlet states spread out into a band while the triplet band width has virtually no splitting. In general, two types of aggregation, J and H, are encountered according to the θ angle between the transition dipole moment and the axis interconnecting the center-of-mass of two adjacent molecules

(see Figure 5a). An indication on the aggregation type can be also inferred, when information on the transition dipole moment is not available, from the distance between centroids of the interacting units. The borderline between the two aggregation modes corresponds to the relative arrangement where the dipole-dipole interaction is null, that is $\theta = 54.7^\circ$. Larger (smaller θ values are associated to H (J) aggregation modes. In particular, a perfect H-aggregate corresponds to the parallel face to face orientation of the transition dipole moments ($\theta = 90^\circ$). According to the Kasha model, in this case transitions from (to) the bottom of the exciton band to (from) the ground state are forbidden since they do not produce any variation in the transition moment, as sketched in Figure 5b for a H-dimer. The main photophysical processes occurring between singlet and triplet states in H-aggregates are shown in Figure 5b and can be simplified as follows: after photon absorption the electron is promoted to the top of the exciton

band and undergoes a fast IC relaxation to the bottom of the band. Since recombination to the ground state is forbidden, the bottom of the exciton band acts as an energy trap and ISC to energetically close triplet states becomes competitive with the relaxation to the ground state. In fact, ISC is higher in the aggregate, with respect to the monomer, thanks to the smaller ΔE_{ST} value induced by the lowering of the exciton band. For these reasons in H aggregates triplet states are efficiently populated ($k_{ST} \geq k_F$) and phosphorescence can be enhanced with respect to fluorescence.^{40,41}

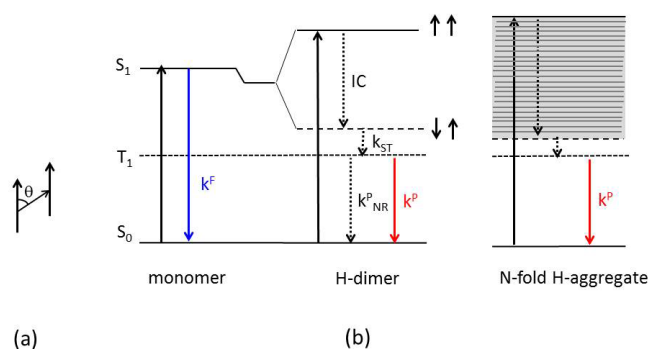


Figure 5. a) Transition dipoles orientation in a molecular aggregate; b) Scheme of the main photophysical processes occurring between the ground state and the first singlet and triplet excited states for a monomer and a H-dimer (or N-fold H-aggregate) with face to face orientation, $\theta=90^\circ$. Phosphorescent emission in H-aggregates is a consequence of the favored ISC induced by small ΔE_{ST} and small k_F ($k_{ST} \geq k_F$) combined with the reduction of non-radiative triplet state deactivations ($k_{PNR} \leq k_P$) accomplished by the crystal packing.

H-aggregation can be effective in realizing organic afterglow at room temperature due to the intrinsic long lifetimes of triplet states in organics (small k_P) combined with reduction of non-radiative deactivation processes of the stabilized triplet state ($k_{PNR} \leq k_P$).

In 1978 Bilen et al.² were the first to report on the unusual afterglow emission of some crystalline organic derivatives. In that early report, the authors specifically focused on crystalline carbazole (Cz), **7**, which produces a weak yellow afterglow ($\lambda_{em} = 568, 552 \text{ nm}$, $\tau = 0.7 \text{ s}$) distinctly different from the compound's molecular phosphorescence (measured in n-heptane at 77K or in a thermoset resin at RT at $\lambda_{em} \approx 450 \text{ nm}$, $\tau = 4.5 \text{ s}$). The authors proposed that the afterglow was produced from the deactivation of an excited triplet state of a dimer or Cz pair. It is really interesting to note that this very pioneering paper has received very little attention in the past with only one citation by the same authors in 1978,⁴² one in 2006,⁴³ two in 2016,^{21,44} three in 2017^{3,45,46} and already one in 2018⁴⁷ testifying the growing interest in organic RTUP.

It took 40 years to have other authors reinvestigating in 2018 the ultralong emission of crystalline Cz in relation to that observed for iminodibenzyl, **8**.⁴⁷ In particular, this very recent study was performed by Sun et al. in view of their previous results (see later).⁴⁸ They were in fact the first to propose to exploit the ability of H-aggregates in the stabilization of the triplet excited states in order to increase the lifetime of phosphorescence of organic materials.

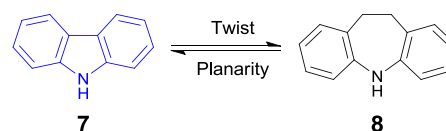


Chart 2. Compounds **7** and **8**.

In the 2018 paper⁴⁷ the authors compare the photoluminescent behavior of Cz **7** and iminodibenzyl **8** with the aim of finding a relationship between molecular conformation and the compounds' RTUP property. In opposition to **7** having a conjugated, planar molecular structure, **8** possesses an unconjugated, twisted conformation due to the presence of the additional C-C bond. Both compounds display in diluted 2-methyltetrahydrofuran solution at 77 K an emission in the range 400-500 nm attributed to phosphorescence in agreement with PL spectra recorded with 5 ms delay. However, while the phosphorescence of **7** is not affected by the excitation wavelength, that of **8** shifts from 403 to 497 nm on moving λ_{ex} from 290 to 370 nm. Supported by DFT calculations, the authors associated this phenomenon to the presence at RT of different twisted conformations with various lowest triplet states. By cooling at 77 K such conformations are instantly fixed in solution, forming single molecules at different energy levels.

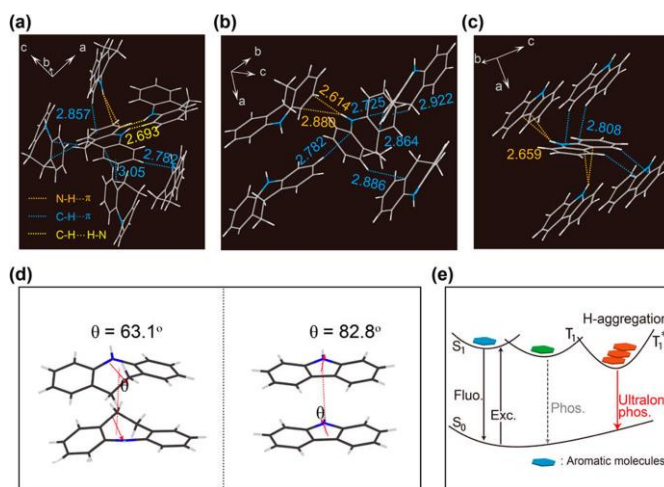


Figure 6. Crystal packing of **8** (a and b) and **7** (c). (d) H-aggregates of **8** and **7**. (e) Schematic diagram of H-aggregated molecules stabilizing triplet excitons for organic RTUP. (Reprinted with permission from ref. 47. Copyright 2018, American Chemical Society).

Crystalline **7** and **8** display concomitant fluorescence, delayed fluorescence by triplet-triplet annihilation (TTA) and RTUP, all of which are blue-shifted for the not conjugated **8** with respect to conjugated **7**, resulting in a green afterglow ($\lambda_{em} = 520 \text{ nm}$, $\tau = 402 \text{ ms}$) for the former and a yellow one ($\lambda_{em} = 560 \text{ nm}$, $\tau = 910 \text{ ms}$) for the latter. Single crystal XRD analyses for both compounds revealed multiple intermolecular interactions (including N-H $\cdots\pi$, C-H $\cdots\pi$ and N-H \cdots H-C) and formation of H aggregates which can stabilize the triplet excitons to realize RTUP under ambient conditions (see Figure 6). The relative

shorter phosphorescence lifetime of **8** with respect to **7** was interpreted as due to looser crystal packing of the former. Additional articles have been reported on RTUP in derivatives containing a Cz unit which, thanks to its planar conjugated structure may favor the formation of H-aggregates in crystals. Particularly successful is Cz functionalization with triazine moiety which, due to the three N atoms, is useful to build multiple interactions in crystals that help in rigidifying molecular conformations.

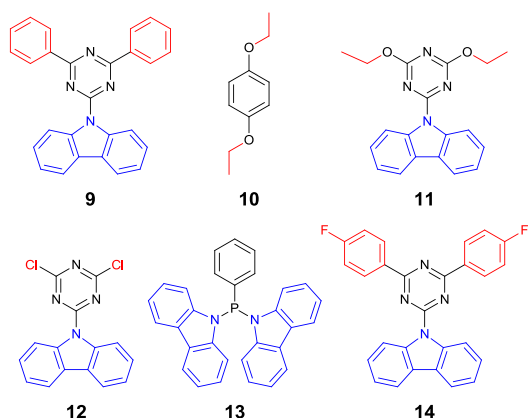


Chart 3. Cz derivatives 9-14.

In 2015, An et al.⁴⁸ performed a deep photophysical investigation on 4,6-diphenyl-2-carbazolyl-1,3,5-triazine (**9**) for which single-crystal XRD analysis revealed the presence of H-aggregates (angle between the transition dipoles and interconnected axis $\theta = 80.9^\circ$, see Figure 7a, c). Upon UV irradiation, powders of **9** display an intense blue fluorescence ($\lambda_{em} = 400-500$ nm; $\tau < 20$ ns and a delayed fluorescence component of $\tau \approx 500$ ms) together with ultralong phosphorescence ($\lambda_{em} = 530$ and 575 nm, $\tau > 1$ s) with $\Phi_p \approx 1.25\%$. In addition, almost identical steady-state photoluminescence spectra and lifetime measurements were obtained in different media (oxygen, argon and ambient atmosphere), revealing an inertness of the triplet excited states to oxygen. Long-lived luminescence (>0.46 s) was also observed in mixed THF/water solution for which the formation of H-aggregates was confirmed by the gradual appearance of a blue shifted absorption peak upon increasing the water content. TDDFT calculations were performed on both singlet and triplet excited states for the isolated molecule and aggregated structures. It was found that the lowest singlet and triplet excited states of the monomer are considerably close (<0.3 eV), facilitating S-T ISC. In addition, while four main ISC transitions from S_1 to T_n were calculated for the monomer, an increased number of S_1-T_n energy transition channels were determined for the aggregate indicating an enhanced ISC probability for the latter. As depicted in Figure 7, the high SOC provided by the $n-\pi^*$ character of the transition derived from N atoms in **9** contributes to populate the triplet states through S-T ISC. H-aggregation stabilizes the triplet excitons (T_n^*) so that their extended lifetime is responsible of the observed RTUP. To test the general validity of their approach, the authors then extended their investigation to solid 1,4-dimethoxybenzene (**10**), 4,6-dimethoxy-2-carbazolyl-1,3,5-triazine (**11**), 2-carbazolyl-4,6-

dichloro-1,3,5-triazine (**12**) and di(9H-carbazolyl)-phenylphosphine (**13**). All compounds exhibit long triplet lifetimes (from 0.21 to 1.35 s) resulting in RTUP able to produce a marked change in the color of the glowing background, from the prompt fluorescence dominating the steady state emission, to the phosphorescence.

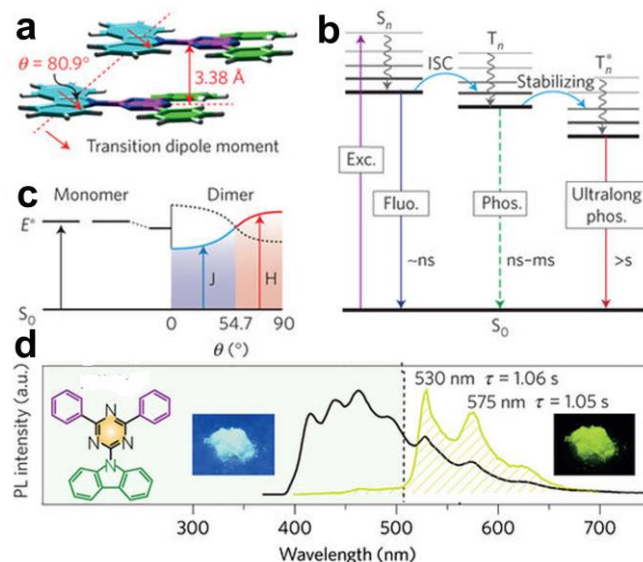


Figure 7. a) Single-crystal structures of **9** showing the formation of H-aggregates as evident by the θ angle; b) Scheme of the main processes for fluorescence (Fluo.), phosphorescence (Phos.) and ultralong phosphorescence (Ultralong phos.) in aggregates of **9**; c) Schematic energy diagram of J-aggregation ($\theta < 54.7^\circ$) and H-aggregation ($\theta > 54.7^\circ$) with blue and red solid curves representing the exciton energy levels of allowed transition for J- and H-aggregation, respectively; d) The steady-state photoluminescence (left) and ultralong phosphorescence (right) spectra of **9** with the corresponding photographs taken before (left) and after (right) the excitation source is turned off. (Adapted with permission from ref. 48. Copyright 2015, Springer Nature).

Later on, some of the same authors reported a deep investigation on the synthesis and proof-of-concept application of organic semiconducting nanoparticles (OSNs) with RTUP for in vivo afterglow imaging.⁴⁹ Water-soluble OSNs of the previously reported phosphorescent **9** and **12** dyes, and the new 4,6-bis(4-fluorophenyl)-2-carbazolyl-1,3,5-triazine (**14**) were synthesized in water by using an amphiphilic triblock copolymer, PEG-b-PPG-b-PEG, to stabilize nanoparticles in water during the sonication for both bottom-up (nanoprecipitation in solution) and top-down (direct conversion of solid dyes into the water-soluble nanoparticles) approaches. The formation of H aggregates within OSNs obtained by both strategies was confirmed by the appearance of a new blue shifted absorption peak. In addition, the broader absorption peak and the larger size of OSNs obtained through the top-down approach were associated to a stronger extent of molecular packing. In agreement with the higher tendency towards H aggregation, OSNs prepared with the top-down approach better stabilize the triplet excitons resulting in longer phosphorescence lifetimes (close to 1s and detectable even 10 seconds after removal of the excitation source) with respect to

those prepared by the bottom-up procedure for all three dyes. In addition, the RTUP is inert to oxygen and water and can be repeatedly activated, making it suitable for long term imaging in living animals, as validated in living mice by the authors by using OSNs dye **9** prepared by the top-down approach.

Very recently, Gu et al.⁵⁰ prepared and investigated three other compounds containing a triazine core, alkyl chains with different hetero atoms (C, N and O) and with double Cz units, namely 9,9'-(6-propyl-1,3,5-triazine-2,4-diyl)bis(9H-carbazole) (**15**), 4,6-di(9H-carbazol-9-yl)-N-ethyl-1,3,5-triazin-2-amine (**16**) and 9,9'-(6-ethoxy-1,3,5-triazine-2,4-diyl)bis(9H-carbazole) (**17**), that display RTUP with lifetime above 630 ms. In dilute chloroform solution at RT, quite intense emission of intramolecular charge transfer (ICT) character is observed for all compounds (**15**: $\lambda_{em} = 430$ nm, $\Phi = 9.7\%$; **16**: $\lambda_{em} = 401$ nm, $\Phi = 15.4\%$ and **17**: $\lambda_{em} = 419$ nm, $\Phi = 9.2\%$). The crystalline dyes exhibit white persistent luminescence (overall Φ reaching 45.8%) due to the presence of both delayed fluorescence resulting from TTA ($\lambda_{em} \approx 400$ -450 nm) and bright yellow RTUP ($\lambda_{em} \approx 540$ nm) which can last for more than 5 seconds ($\tau = 632$, 650 and 789 ms for **17**, **15** and **16** respectively).

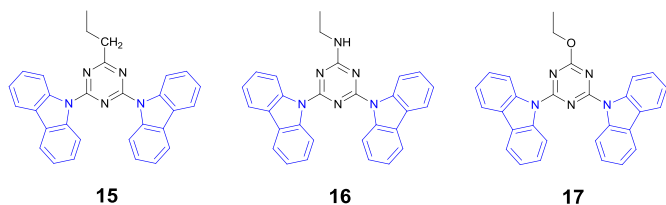


Chart 4. Cz-triazine derivatives **15-17**.

TDDFT calculations indicated a high number of S_1 - T_n energy transition channels for the aggregate suggesting a high ISC probability. Single-crystal XRD revealed for all three compounds the presence of a large number of intra/intermolecular interactions (i.e. C-H \cdots π and C-H \cdots N) together with formation of H aggregates which were considered responsible of the observed RTUP (see Figure 8).

Moreover, the authors attributed the prolonged lifetime of the RTUP of **16**, which possesses an extra-N atom, to the synergic presence of polar dihydrogen bonding (C-H \cdots H-N) which contributes in rigidifying the molecular conformation thus restricting non radiative transitions (see Figure 8).

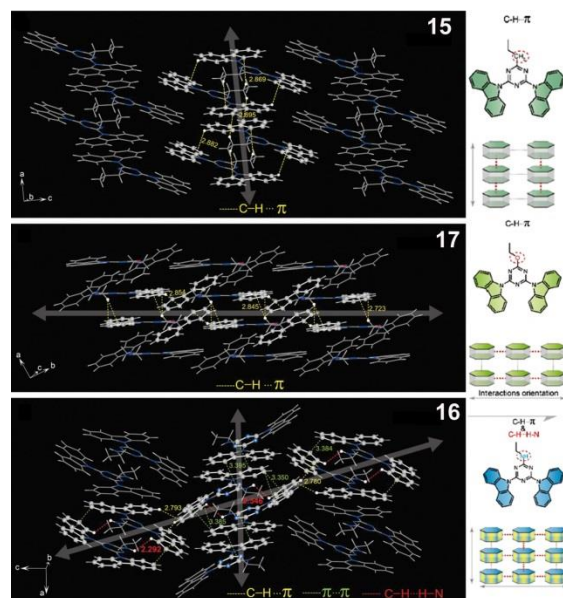
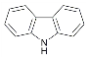
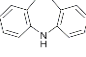
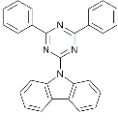
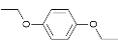
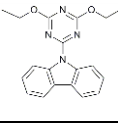
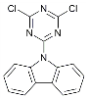
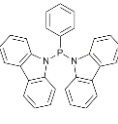
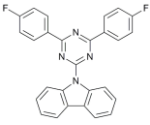
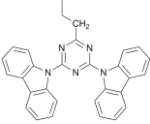
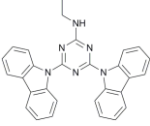
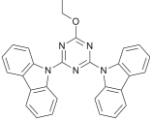


Figure 8. Left: Molecular stacking in crystals of **15**, **17** and **16**. The orientations of intermolecular interactions are highlighted by double sided arrows. Right: Schematic diagram of the dominant intermolecular interactions in solid states. (Adapted from ref. 50 with permission from The Royal Society of Chemistry).

Table 2 RTP Emission Maxima (λ_{em}), Phosphorescence Quantum Efficiency (Φ_p), and Lifetimes (τ) of compounds **7-17**

Compound		Phosphorescence			Reference
Label	Structure	λ_{em} (nm)	Φ_p (%)	τ (ms)	
7		522, 552, 568, 600, 625	n.d.	700 ^a 880 ^b	2
		560	n.d.	910	47
8		520	n.d.	402	47
9		530 575	1.25	1066 1052	48
9-SNs		530	1.77	861	49
10		515 547	0.3	710 692	48
11		529 574	0.6	1282 1347	48
12		543 591	2.1	471 491	48
12-SNs		530	1.86	354	49
13		587 644	0.08	210 290	48
14-SNs		530	3.50	440	49
15		546	1.36	650	50
16		543	1.70	789	50
17		553	1.63	632	50

^a measured at 552nm; ^b measured at 568nm

Cz has also been used as electron donor (D) unit in some organic non-planar Donor-Acceptor (D-A) derivatives for which crystal-phase RTUP has been reported and interpreted in terms of their crystal packing. In the 4-(9H-carbazol-9-yl)benzaldehyde (**18**) prototype proposed by Xue et al.,⁵¹ benzaldehyde was used as Acceptor (A) unit, where the carbonyl oxygen could generate an intrinsic triplet state through ISC. As expected on the basis of its D-A structure, **18** dissolved in solvents of different polarity displays a red-shift of the absorption and emission bands, ascribable to twisted intramolecular charge transfer (TICT) character of the transition. In particular, on the basis of TDDFT calculations, the $S_0 \rightarrow S_1$ transition was described mainly as (π, π^*) HOMO \rightarrow LUMO transition, with HOMO and LUMO principally distributed on Cz and benzaldehyde, respectively. However, contrary to the general observation that ICT molecules are strongly fluorescent in nonpolar solvents and weakly fluorescent in polar solvents, **18** emits very weak fluorescence in cyclohexane ($\lambda_{em} = 370$ nm, $\Phi = 0.048$) and stronger fluorescence in CH_2Cl_2 ($\lambda_{em} = 478$ nm, $\Phi = 0.28$). This anomalous behavior was ascribed to different ISC efficiency of **18** in solvents with different polarity. In fact, polarized continuum model (PCM) TDDFT calculations in cyclohexane and CH_2Cl_2 indicated that in the former solvent a triplet state of (n, π^*) character, T_3 , lies slightly below S_1 . This grants efficient ISC thanks to both the small S-T band gap and the different character of the involved excited states, implying weak fluorescent emission. On the other hand, in CH_2Cl_2 , T_3 lies above S_1 owing to the energy decrease of the n orbital, and T_2 has (π, π^*) character, thus preventing ISC and favoring strong fluorescence. Owing to the (π, π^*) configuration of T_1 , cyclohexane solutions of **18** are expected to be phosphorescent and they are so only at 77 K ($\lambda_{em} = 454$ nm, $\tau = 95$ ms), thanks to the suppression of intramolecular motions. Moving to solid state, both as-synthesized solids and crystals of **18** revealed two groups of emission ($\Phi = 9\%$). In particular, for crystals, one is attributed to fluorescence ($\lambda_{em} = 439$ nm, $\tau = 1.9$ ns) and TADF ($\lambda_{em} = 444$ nm, $\tau = 130$ ms) and the other to RTUP ($\lambda_{em} = 550$ nm, $\tau = 540$ ms). The red-shift of the phosphorescent emission with respect to the 77 K solution was related to molecular aggregation, and in particular to π - π interactions. Single-crystal XRD studies on **18** revealed in fact the presence of head-to-tail H-dimers (see Figure 9) where the benzene rings are placed at interplanar distance of 3.257 Å. Owing to the large twist angle between the Cz and the benzaldehyde moieties (47.77°), the benzene rings undergo a relatively large lateral shift, as denoted by the distance between their centroids (5.380 Å). Additionally, C-H \cdots π hydrogen bonds contribute to suppress intramolecular motions reducing the non-radiative deactivation channels. Interestingly, the compound revealed also reversible conversion from phosphorescence to fluorescence through mechanical stimulus. Thorough grinding, in fact, leads to amorphous solid where phosphorescence disappears owing to the free rotation and vibrational motions, resulting in only blue fluorescence. RTUP is rapidly restored within 2 min, suggesting that the amorphous solid is unstable and converts into the stable crystalline state.

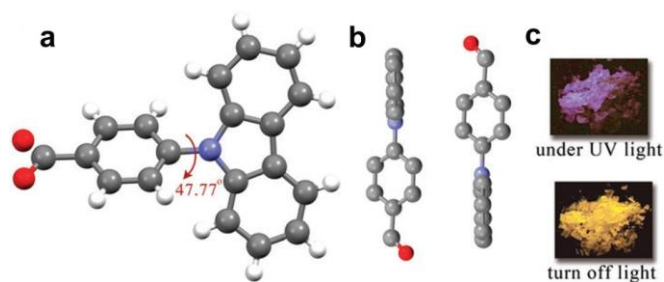


Figure 9. a) Molecular structure and b) packing structure between molecules of **18** in crystals; c) photos of crystals under 365 nm light and then after turning the light off. (Adapted from ref. 51 with permission from The Royal Society of Chemistry).

Another example of D-A derivatives showing RTUP in crystal phase is (9H-carbazol-9-yl)(phenyl)methanone (**19**).^{52,53} This chromophore displays in dilute chloroform solution at RT absorptions at 279, 305, and 315 nm. The PL spectrum shows an emission band with fine vibrational structures at 343 and 356 nm and a broad unresolved band at 524 nm. The former is slightly affected by the solvent polarity and corresponds to the locally excited state while the latter exhibits a bathochromic shift with increasing solvent polarity, in agreement with its ICT character.⁵² At 77 K the phosphorescence spectrum displays a structured long lasting emission (with onset at 403 nm)⁵³ associated with the suppression of the nonradiative decay of triplet excited states in such a rigid frozen environment.⁵²

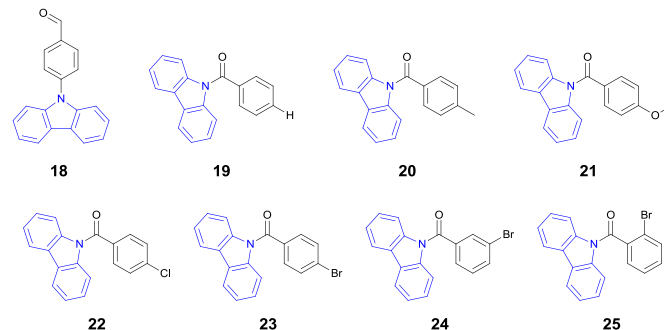


Chart 5. D-A Cz derivatives **18-25**.

Xie et al.⁵³ compared the photophysical behavior of **19**, (9H-carbazol-9-yl)(*p*-tolyl)methanone (**20**) and (9H-carbazol-9-yl)(4-methoxyphenyl)methanone (**21**) which display identical optical properties in solution both at RT and 77 K. However, quite different emissive properties are shown by their crystals due to different packing arrangement. In particular, on the basis of single crystal XRD and DFT/TDDFT calculations, the authors suggested that the close face to face packing plays a critical role not only in stabilizing the singlet excited state, but also in facilitating the intermolecular coupling and the stabilization of the triplet exciton. In agreement, **19**, with the tightest face to face arrangement (N-N distance of 5.53 Å), possesses the strongest PL efficiency (3.17 %) and the longest RTP lifetime (748 ms at 530 nm) (see Figure 10). The looser packing of **20** and

21 (N-N distance of 6.02 and 6.17 Å respectively) results in a gradual decrease of PL efficiency and RTP lifetime (1.98, 0.51%; 340 ms at 540 nm and 114 ms at 545 nm, for **20** and **21**, respectively). The gradual blue-shift in the PL emission on going from **19** to **20** and **21** ($\lambda_{em} = 445, 442$ and 425 nm, respectively) was associated with the weakened electron withdrawing ability of the benzoyl group in the presence of the methyl and methoxy substituent.

Further confirmation of the importance of a compact packing for the optimization of the emissive performances was obtained by analyzing a different polymorph of **19**, **19-A**, with very similar but slightly looser packing than that of **19** (interplanar distance equal to 3.49 vs. 3.45 Å), which shows drastically decreased RTP intensity and lifetime (63 ms, $\lambda_{em} = 540$ nm)(see Figure 11).

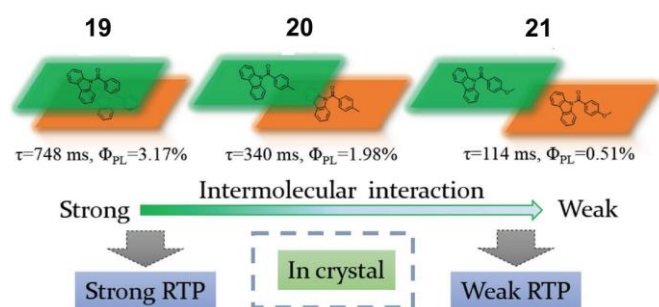


Figure 10. Cartoon modes for crystal packing of **19**, **20** and **21**. (Adapted with permission from ref. 53. Copyright 2017, Wiley-VCH Verlag GmbH & Co. KGaA).

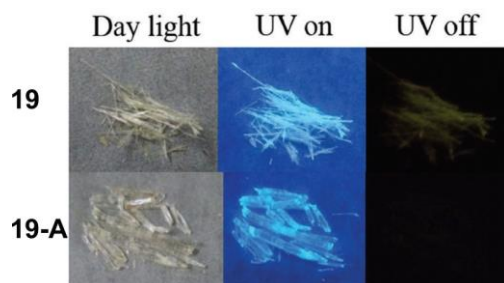


Figure 11. Pictures of **19** and **19-A** crystals under day light, ultraviolet source (365 nm) and after removal of UV. (Adapted with permission from ref. 53. Copyright 2017, Wiley-VCH Verlag GmbH & Co. KGaA).

In 2017, Cai et al.⁵² compared the photophysical behavior of **19** and its halogenated derivatives, namely (9H-carbazol-9-yl)(4-chlorophenyl)methanone (**22**) and (9H-carbazol-9-yl)(4-bromophenyl)methanone (**23**). At RT, powders of **19**, **22**, and **23** exhibit blue, blue-green, and yellow-green emission respectively under 365 nm excitation, and ultralong yellow-green luminescence (τ over 0.63 s for **19** and **23**, and over 0.82 s for **22** for which Φ_p reached 8.3%). For the three compounds dispersed in PMMA matrix, ultralong phosphorescence is observed only at 77K in agreement with rigidification effects. DFT calculations on molecular stacking models selected from single crystal structures (see Figure 12) revealed the presence of synergic intermolecular interaction in different

dimensionalities. In particular, for the three compounds, the RTUP is achieved through H-aggregation (along the z-axis) which stabilizes and protects the excited triplet state by the strong coupling of π - π stacking (the UP features of **22** are ascribed to two types of H-aggregates in its structure). In addition, while the halogen substituents have no influence on triplet excited states of the isolated molecules (in agreement with the identical phosphorescence spectra of the three compounds in frozen solutions), Cl/Br...H-C interactions between neighboring molecules in the xy plane are involved in the absorption red-shift of **22** and **23** so that the two compounds can be excited by using visible light. Impressively, powders of **22** can be excited by easily accessible light-emitting diode (LED) light sources (i.e. mobile phone flashlights or incandescent light). Water-soluble NPs of **22** encapsulated by an amphiphilic triblock copolymer of PEG-b-PPG-b-PEG were prepared by a top-down method. The NPs showed good aqueous solubility and ultralong phosphorescence (τ equal to 0.65 s) and their potentiality in bioimaging applications was demonstrated.

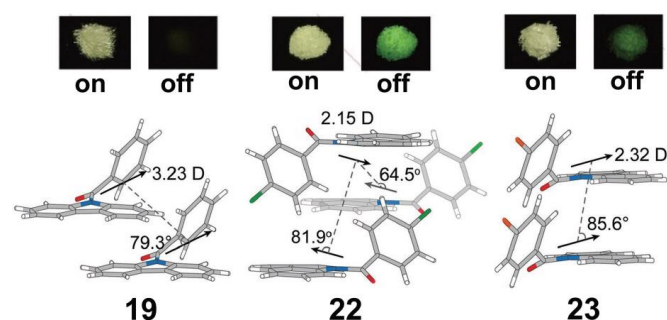
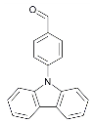
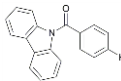
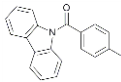
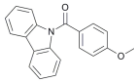
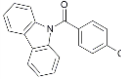
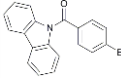
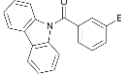
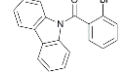


Figure 12. Top: Photographs of **19**, **22**, and **23** under 365 nm UV light on and off; Bottom: Dimers of **19**, **22**, and **23** in single crystals showing formation of H-aggregation. The transition dipole moments and measured angles between transition dipoles and interconnected axis are shown. (Adapted with permission from ref. 52. Copyright 2017, Wiley-VCH Verlag GmbH & Co. KGaA).

Later on, Liu et al.⁴⁶ performed a full investigation on the three regioisomers of (9H-carbazol-9-yl)(bromophenyl)methanone with bromo substitution on the phenyl ring in para- (**23**), meta- (**24**) and ortho- (**25**) position. While diluted solutions of the three compounds at cryogenic temperature display identical phosphorescence spectra (arising from the Cz moiety), the emission of the crystals shows important differences that depend on the crystal quality. In particular, crystalline **23** ($\Phi = 18\%$), which is a polymorph of the one displaying RTUP previously reported by Cai et al.,⁵² displays a broad TADF ($\lambda_{em} = 473$ nm, having a prompt component with $\tau = 1.62$ ns, and a delayed component with $\tau = 3.4$ ms) but no RTP. Crystals of the two other regioisomers, **24** ($\Phi = 5\%$) and **25** ($\Phi = 12\%$), exhibit both fluorescence ($\lambda_{em} = 444$ nm with $\tau = 1.13$ ns and $\lambda_{em} = 438$ nm with $\tau = 2.61$ ns for **24** and **25** respectively) and RTP with well resolved peaks at 529, 575, 629 nm (with τ equal to 211 and 208 ms for **24** and **25** respectively). Moreover, **24** shows RTP emission peaked at 472 nm (206 μ s).

Table 3 RTP Emission Maxima (λ_{em}), Phosphorescence Quantum Efficiency (Φ_p), and Lifetimes (τ) of compounds **18-25**

Compound		Phosphorescence			Reference
Label	Structure	λ_{em} (nm)	Φ_p (%)	τ (ms)	
18		550	n.d.	540	51
19		530	n.d.	748	53
		530	0.7	646	52
20		530	n.d.	340	53
21		550	n.d.	114	53
22		570	8.3	847	52
23		536	3.4	667	52
24		529, 575, 629	n.d.	211	46
25		529, 575, 629	n.d.	208	46

Such an intriguing behavior is ascribed to the different ways of triplet exciton harvesting occurring in the three crystalline regioisomers, that finely depends on the intermolecular electronic interactions imposed by different π - π stacking modes and overlapping molecular orbitals. Single crystal XRD analysis was performed in order to get information on the packing motifs (see Figure 13 left). It was found that substitution with bromine in different positions leads to different torsion degrees of the benzoyl ring with respect to the Cz unit producing different crystalline arrangements. However, bromine atom is only marginally involved in the self-assembling

of the three regioisomers. In fact, a weak C-H \cdots Br hydrogen bonding and an inter-halogen C-Br \cdots Br-C type-I contact are observed in **23** and **25**, respectively, while no contact with bromine is present in **24**. It is then expected that, while promoting SOC as a heavy atom, bromine does not play a role in switch-on RTP from these aggregates. More important appear to be C-H \cdots π hydrogen bonds and π - π stacking interactions connecting centro-symmetry-related molecules to form head-to-tail and slipped parallel dimers. In particular, π - π stacking interaction occurs between Cz rings in **23** (stacking distance equal to 3.39 Å) and benzene rings in **24** and **25**

(stacking distances equal to 3.39 and 3.51 Å, respectively). The lateral displacement of one monomer with respect to the other within dimers is much greater in **23** with respect to **24** and **25**, as denoted by the distances between centroids of carbazoles in **23** (5.74 Å) and those of benzene rings in **24** (3.75 Å) and **25** (3.79 Å). This is, in our opinion, a first indication to rationalize the RTUP emission displayed by **24** and **25**. The little lateral displacement of the interconnected π - π units in these structures suggests in fact that they can be described as almost face-to-face H-dimers, whose presence, as mentioned above, has been elsewhere invoked to explain RTUP.⁴⁸ Moreover, in the crystal structure of **24** the carbonyl oxygen of one monomer is as close as 3.06 Å (3.04 Å from DFT calculations on optimized dimeric models) to a carbon atom of the phenyl ring of the interacting monomer, a distance well below the sum of the oxygen and carbon van der Waals radii (3.2 Å). This further indicates strong intermolecular electronic coupling within the dimer. DFT calculations on dimeric models extracted from the

crystal structure provided in all cases relatively high binding energies (> 11 kcal/mol), confirming that the identified head-to-tail and slipped parallel arrangements are strongly bound to each other. By means of TDDFT calculations on the optimized dimeric models, the authors evaluated the effect of the intermolecular interactions on the singlet and triplet energy levels, thus elucidating the triplet harvesting mechanism involved in the different crystals (see Figure 13 right). In particular, the separated HOMO-LUMO distribution and the little S_1 - T_2 separation (0.06 eV) computed for the slipped-parallel dimer of **23** explains its observed delayed fluorescence. On the other side, based on the matching between computed and observed energy levels, the two distinct dimeric units individuated in **24** are inferred to be responsible for fluorescence and RTP independently (slipped-parallel dimer) and for RTUP (head-to-tail dimer), respectively, while the slipped-parallel dimer of **25** is speculated to be the emissive species of RTUP.

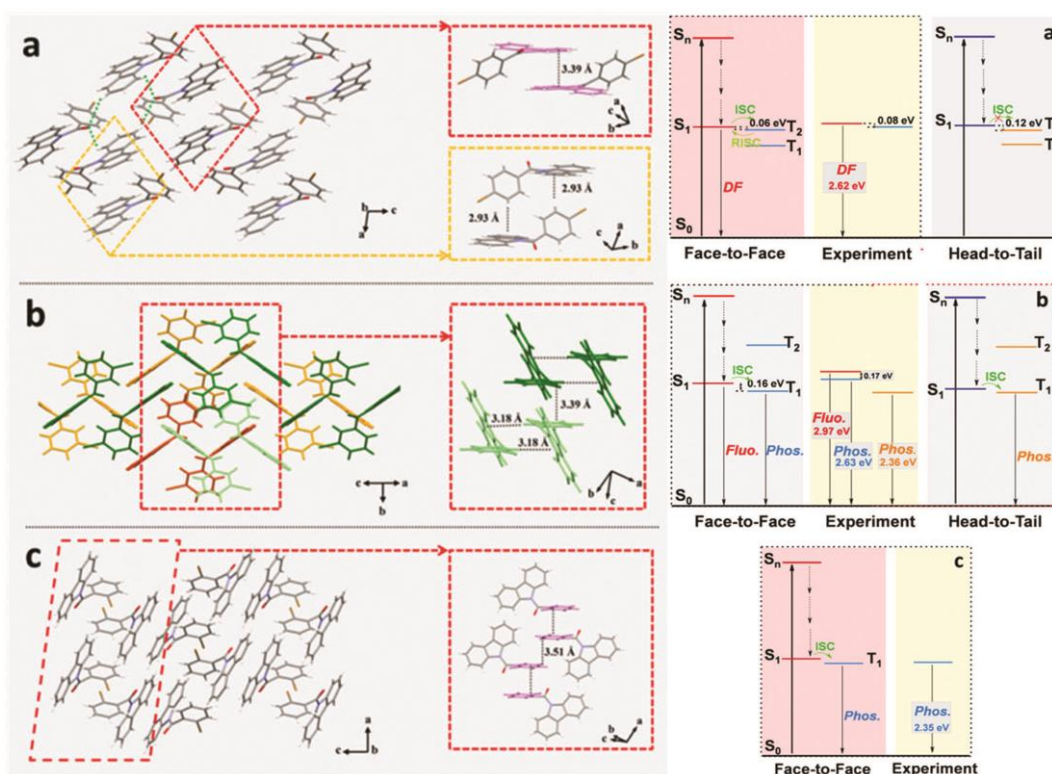


Figure 13. Left: Packing motifs and intermolecular interactions of **23** (a), **24** (b) and **25** (c) evidencing slipped-parallel and head-to-tail dimers; Right: A comparison of excited state structures between computational results and experimental values, following the **23** (a), **24** (b) and **25** (c) sequence. (Adapted from ref. 46 with permission from The Royal Society of Chemistry).

The idea to use Cz as electron donor moiety in Donor-Acceptor luminescent compounds has been extensively developed also by Gong et al.⁵⁴ In particular, the authors proposed a design strategy based on the use of D-A compounds with comparable molecular size of the constituent subunits. This feature was in fact expected to satisfy the requirement of strong intermolecular interactions in crystal phase, able to constrain intrinsic nonradiative decays (i.e. C-H stretching vibrations)

generating smaller k_{nr} and thus longer τ_p . In this regard, the authors fully characterized (4-(9H-carbazol-9-yl)phenyl)(phenyl)methanone (**26**), a D-A compound based on Cz and Bp as the electron acceptor unit. Indeed, crystals of **26** display simultaneous prompt fluorescence, delayed fluorescence and RTUP ($\tau = 517.87$ ms) associated with a 3D intermolecular network with several short C-H \cdots O, C-H \cdots π and H \cdots H contacts (see Figure 14). In the crystal structure of **26** also

relatively strong π - π interactions between Cz units are observed, which form infinite columns with distances between Cz planes and centroids alternately equal to 3.52, 3.79 Å and 3.32, 4.68 Å, respectively. The whole body of such interactions are responsible of a dense crystal packing which, according to the authors, generate highly rigidified molecular conformations and are able to protect from humidity and oxygen. Due to the blue fluorescence combined with the orange phosphorescence, **26** resulted as white light emitter.

To support their interpretation, the authors prepared and characterized the mono- (**27**) and di-bromo (**28**) derivatives of **26** bearing the halogen on the Cz unit. The two compounds display relatively short τ_P (0.11 and 0.16 ms for the mono- and di-bromo derivative respectively) which were ascribed to looser crystal packing and vigorous vibrational dissipations rather than heavy atom effect. In fact, single crystals of **27** cannot be obtained and the crystal structure of **28**, while displaying several short contacts, is characterized by weaker π - π interactions between Cz units (the distances between Cz planes and centroids are equal to 3.59 and 3.91 Å, respectively) with respect to **26**. In agreement with such hypothesis, long lasting phosphorescence was observed for crystals of the two compounds only at cryogenic temperature. Moreover, transformation between crystalline and amorphous states through mechanical grinding was accompanied by the disappearance of triplet emissions for the three compounds.

Further investigation on the mechanism involved in the RTUP of **26** was performed by Yang et al. in 2016.⁴⁴ The authors observed that a common feature of different RTUP organic molecules with D-A twisted structure reported in the literature is the presence of units with different excited-state configurations (i.e., $n\pi^*$ and $\pi\pi^*$) and close intermolecular interactions due to the strong electrostatic interactions between these units. Based on these two factors, a new mechanism to explain organic RTUP was proposed which involves not only the presence of a crystalline rigid state able to insulate from oxygen in the air but also of hybrid ISC transitions generated through intermolecular electronic coupling (IEC) of units with partial orbital overlapping.

The hybrid nature of these ISC transitions guarantees high k_{ST} derived from the n unit and low k_P rates originating from the π unit resulting in bright RTUP (see Figure 15). Moreover, because of the twisted configuration between D and A moieties as observed in **26**, the spatial overlap between HOMO and LUMO is reduced. This originates a small energy gap between S_1 and T_1 excited states, facilitating the ISC process. The effectiveness of the proposed mechanism was verified through structural, photophysical and theoretical analysis not only in **26** where the carbonyl is the n unit and the carbazolyl is the π unit, but also in RTUP derivatives containing a sulfonyl group as the n unit.

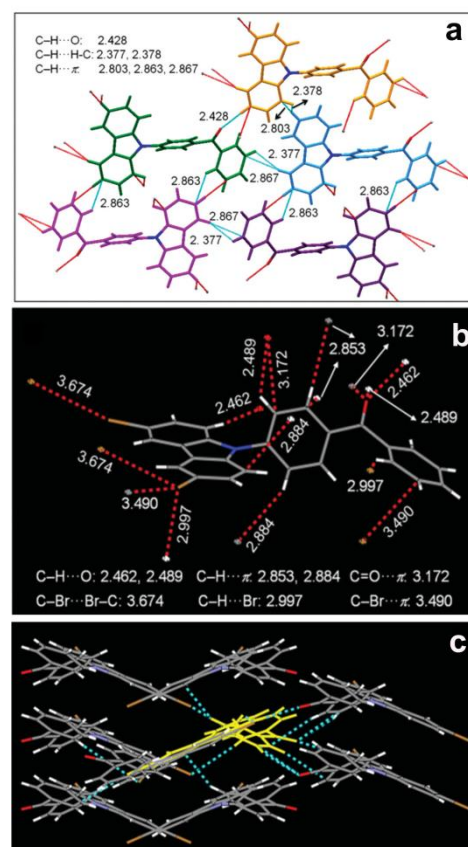


Figure 14. Single-crystal structure and molecular packing of a) **26**, b) and c) **28** with denoted intermolecular interactions. (Adapted with permission from ref. 54. Copyright 2015, Wiley-VCH Verlag GmbH & Co. KGaA).

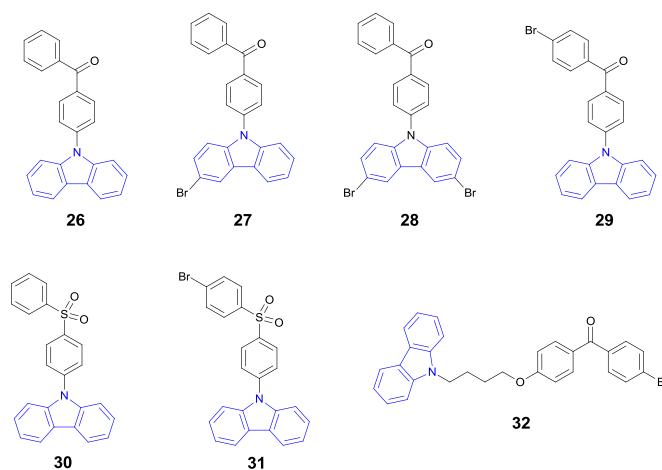


Chart 6. D-A Cz derivatives **26-32**.

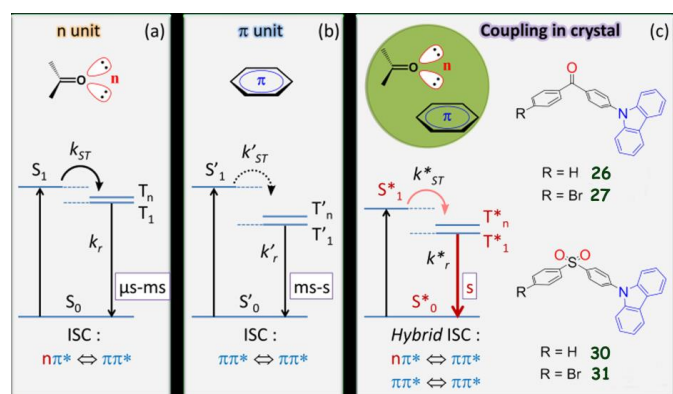


Figure 15. Energy level diagram of the relevant photophysical processes for the phosphorescence of organic molecules with a) $n\pi^*$ excited state configuration (i.e., containing an n unit) and b) $\pi\pi^*$ excited state configuration (i.e., containing a π unit). c) Proposed energy level diagram of the relevant photophysical processes for RTUP of coupled intermolecular n and π units in organic crystals. k_r = radiative rate. (Adapted with permission from ref. 44. Copyright 2016, Wiley-VCH Verlag GmbH & Co. KGaA).

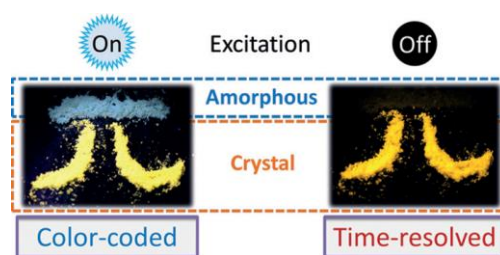


Figure 16. Example of the use of **26** for dual-responsive security protection applications. When excited with ultraviolet irradiation (365 nm) the amorphous part (light blue) of security letter “ π ” is clearly distinguished from the crystal part (yellow). After excitation turn off, only the crystal part (orange) of the letter is visible. (Reprinted with permission from ref. 44. Copyright 2016, Wiley-VCH Verlag GmbH & Co. KGaA).

Table 4 RTP Emission Maxima (λ_{em}), Phosphorescence Quantum Efficiency (Φ_p), and Lifetimes (τ) of compounds **26-32**

Label	Compound Structure	Phosphorescence			Reference
		λ_{em} (nm)	Φ_p (%)	τ (ms)	
26		552, 569, 597	1.4	518	54
		570 624	0.3	479 465	44
27		555	0.3	0.11	54
28		545	7.5	0.16	54
29		549 602	5	287 277	44
30		562	n.d.	394	44
31		558	6	122	44
32		549, 602	11	140	55



In **26**, in particular, the authors identify a close contact between the carbonyl group and the Cz group in a neighbor molecule, with distances with the Cz plane as short as 3.373 Å for the oxygen atom and 3.561 Å for the carbon atom. This stacking mode allows significant spatial overlap of their respective n and π orbitals. According to the authors, this particular packing feature, rather than other interactions, is at the origin of the intense RTUP emission ($\lambda_{em} = 624$ nm, $\Phi_p = 0.3\%$, $\tau = 0.49$ s). This RTUP is switched off in the amorphous state in air due to increased intramolecular motions and the presence of oxygen, but it is turned on in vacuum since intermolecular coupling between different **26** molecules is still present. In addition, diluted solutions of **26** display at 77 K a much bluer emission ($\lambda_{em} = 450, 484$ and 521 nm) with shorter lifetime (90 ms), supporting the idea that intermolecular interactions are at the origin of the RTUP. Interestingly, the mechanoresponsive RTP of these molecules makes them also interesting as smart materials for use in dual-responsive security protection, as shown in Figure 16.

To verify the effect of a heavy halogen atom on the ISC rate, the authors studied the derivative (4-(9H-carbazol-9-yl)phenyl)(4-bromophenyl)methanone (**29**) bearing a bromine atom on the n unit in para position with respect to the carbonyl group. The idea was that being conjugated to the carbonyl group, the bromine atom should promote the ISC process without affecting the low radiative rates of the π unit. In fact, contrarily to the quenching of the emission observed by Gong et al.⁵⁴ by brominating the π unit in **27**, **29** possesses stronger IEC (shorter distances between the n and π units of two neighboring molecules) than that of **26** and enhanced RTP emission ($\Phi_p = 5\%$). An enhanced RTP due to the heavy halogen atom was also found by comparing the compound with the sulfonyl group (9-(4-(phenylsulfonyl)phenyl)-9H-carbazole, **30**) and its brominated derivative (9-(4-((4-bromophenyl)sulfonyl)phenyl)-9H-carbazole, **31**). This observation is in agreement with what previously reported by Mao et al.⁵⁶ in their studies concerning the mechanoresponsive behavior of **30** and its iodinated derivative, even though in this latter work a clear reference to interchromophoric interaction to support RTP emission is not mentioned.

Based on these exciting results, in 2017 some of the same authors⁵⁵ developed a new strategy to promote a more efficient IEC and intermolecular heavy halogen effect by introducing a flexible alkoxy spacer between Cz and 4-bromobenzophenone so as to facilitate the intermolecular interaction between the head of one molecule and the tail of the adjacent one in the crystalline state. Interestingly, (4-(4-(9H-carbazol-9-yl)butoxy)phenyl)(4-bromophenyl)methanone (**32**) is not emissive in solution but quite so in the crystalline state with a

persistent red phosphorescence with Φ_p equal to 11% and lifetime of 0.14 s. The authors also prepared and directly applied nanocrystals with an average size of 180 nm in the bioimaging of breast cancer cells to demonstrate the potential of RTP compounds in the biological world.

He et al.⁵⁷ explored the potential of integrating the archetypal phosphor Bp with dibenzothiophene, Dbt, the latter showing weak dual RT fluorescence/phosphorescence in the crystal state, to achieve pure-phosphorescence single-component white light emitters. Such an important feature could be realized by at least two distinct phosphorescence bands for color mixing. The synthesized compounds dibenzo[b,d]thiophen-2-yl(phenyl)methanone (**33**), dibenzo[b,d]thiophen-2-yl(4-fluorophenyl)methanone (**34**), dibenzo[b,d]thiophen-2-yl(4-chlorophenyl)methanone (**35**) and dibenzo[b,d]thiophen-2-yl(4-bromophenyl)methanone (**36**), where both the carbonyl group and the heavy atom are expected to boost the inherent phosphorescence efficiency of Dbt, display CIE behavior with the required dual phosphorescence: a fast one ($\lambda_{em} \approx 470$ nm, $\tau = 0.06$ -0.71 ms), which was shown to originate from radiative decay from T_2 , and a long-lived one (about 570 nm, $\tau = 104$ -123 ms), due to emission from T_1 (see Figure 17).

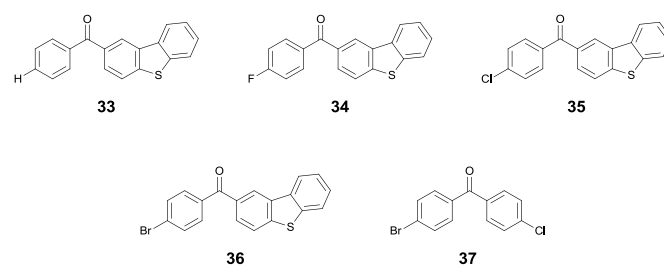


Chart 7. Dbt derivatives of compounds **33**-**37**.

In particular, crystals of **35** exhibit bright white RTP with $\Phi_p = 7.2\%$, while crystals of **33**, **34** and **36** emit yellow ($\Phi_p = 2.3\%$), orange (6.5%) and yellow light (6.8%), respectively. Single crystal XRD of **33**, **35** and **36** revealed the presence of strong π - π stacking interactions between Dbt units for the latter two, which form H-dimers with distances between Dbt centroids equal to 4.225 and 4.206 Å, respectively, and only weaker S...S interactions in **33**, where the Dbt units are largely shifted (see Figure 17). A TADF origin of the short-lived component was excluded on the basis of the observed increased lifetimes with decreasing the temperature. Moreover, TDDFT calculations provided two lowest excited states (T_1 and T_2) below S_1 , with large S_1 - T_1 separation (0.72, 0.88 and 0.74 eV for **33**, **35** and **36**, respectively), suggesting that TADF is less likely to occur at RT.

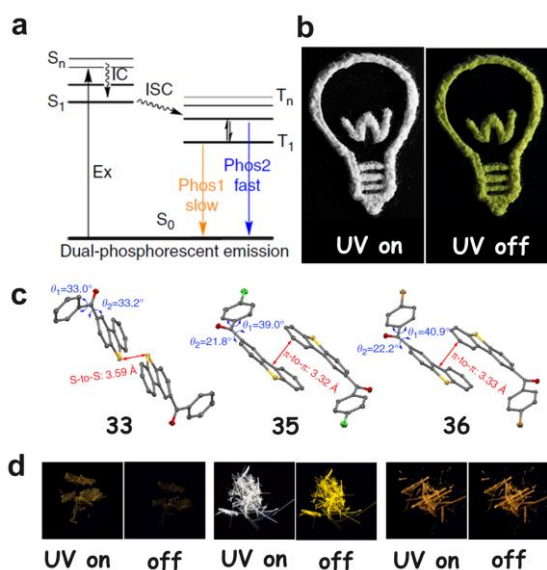


Figure 17. a) Jablonski diagram for dual phosphorescent emission. b) Photo-pattern of **35**. A lamp was drawn using powder of **35**. The white lamp was taken when excitation source is on, the yellow lamp was taken when excitation source is off. c) Crystal structures of **33**, **35** and **36**. d) Photograph of the crystals taken under excitation at 365 nm (UV on) and after excitation was turned off (off) (Adapted with permission from ref. 57. Copyright 2017, Springer Nature).

In addition, though both T_1 and T_2 states have mixed (n,π^*) and (π,π^*) configuration, T_2 is mainly a (n,π^*) transition while T_1 possesses more (π,π^*) character. As a result, according to the El-Sayed rule, a larger SOC is expected between T_2 and S_0 with respect to that between T_1 and S_0 , which leads to short lifetime for T_2 and long lifetime for T_1 . The junction mode between Bp and Dbt, consisting of a shared phenyl group, revealed to be the key point to get the required dual phosphorescence. In fact, Bp mainly contributes to the (n,π^*) transition while Dbt is mainly responsible for the (π,π^*) one. Though the simultaneous RTP from two triplet states T_1 and T_2 is quite unusual, according to the Kasha's rule, it may occur after thermal population of T_2 from the T_1 state if $\Delta E(T_1-T_2)$ is comparable to the thermal energy at RT. Moreover, in order to have a balanced emission from the two states, the radiative decay rate of T_2 should be faster than that of T_1 . The higher-energy T_2 with (n,π^*) transition character and lower-energy T_1 with (π,π^*) transition character fulfill these requests. To further proof this concept the authors studied another halogenated Bp (4-bromo-4'-chlorobenzophenone, **37**) showing cool white light emission and a high $\Phi_P = 28.6\%$ arising from dual RTP emissions from T_1 and T_2 states.

Table 5 RTP Emission Maxima (λ_{em}), Phosphorescence Quantum Efficiency (Φ_P), and Lifetimes (τ) of Dbt and compounds **33-37**

Compound		Phosphorescence			Reference
Label	Structure	λ_{em} (nm)	Φ_P (%)	τ (ms)	
Dbt		546		56.23	57
33		470 567	2.3	0.71 103.7	57
34		465 565	6.5	0.06 106.7	57
35		470 590	7.2	0.41 123.4	57
36		467 570	6.8	0.14 103.8	57
37		425 550	28.6	0.19 19.2	57

The synergistic effect of aromatic carbonyl, promoting ISC, and intermolecular $\pi-\pi$ stacking interactions, stabilizing triplet excitons, has been recently exploited by Cai et al.⁵⁸ to build up efficient luminescent porous hydrogen-bonded organic aromatic frameworks (HOAFs).⁵⁹ The authors designed and

prepared a three-arm Cz derivative, benzene-1,3,5-triyltris((9H-carbazol-9-yl)methanone) (**38**), comprising an aromatic carbonyl core and three π -conjugated Cz groups. According to the crystallization conditions, three types of highly stable HOAFs were obtained, **38-a**, **38-b** and **38-c**, self-assembled through

intralayer π - π stacking interactions and interlayer C-H \cdots O=C hydrogen bonds and characterized by different pore shape and dimensions (see for example **38-b** in Figure 18). While rigidified dilute solutions of **38** and PMMA films (1 wt% of luminophor) at 77K showed two phosphorescence peaks at $\lambda_{em} = 418$ and 447 nm, the three polymorphs exhibited both bright fluorescence ($\lambda_{em} = 516, 506$ and 511 nm with $\tau = 3.9, 3.7$ and 3.8 ns for **38-a**, **38-b** and **38-c**, respectively) and RTP ($\lambda_{em} = 544, 540$ and 540 nm with $\tau = 79.83, 39.9$ and 18.6 ms for **38-a**, **38-b** and **38-c**, respectively). These results, together with observation that both lifetimes and intensities of the phosphorescence decreased by grinding, suggested that intermolecular interactions, rather than RIR of the single molecule, were responsible for the observed RTP. π - π interactions dominate in fact the crystal packing in all the three structures (see for example **38-a** in Figure 18).

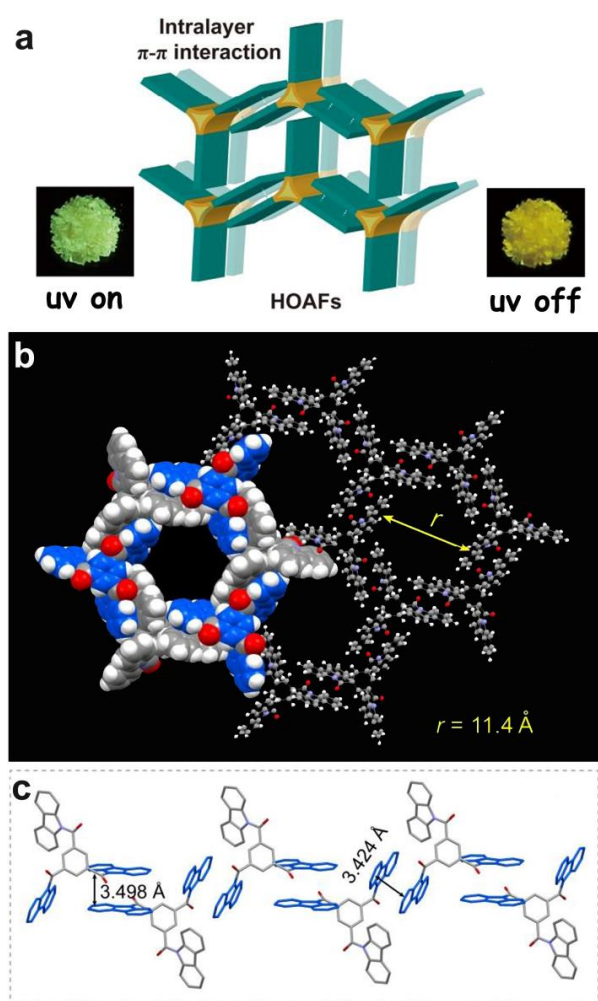


Figure 18. a) Schematic representation of hydrogen-bonded organic aromatic frameworks (HOAFs) based on **38** with photographs of **38-a** under 365 nm UV light on and off; b) Crystal packing of HOAF **38-b**; c) Intermolecular stacking in **38-a** crystal. (Adapted with permission from ref. 58. Copyright 2018, Wiley-VCH Verlag GmbH & Co. KGaA).

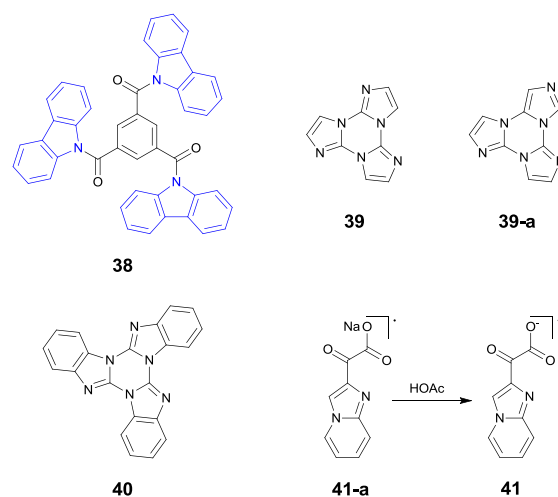


Chart 8. Compounds **38-41**

Other planar molecules displaying RTUP were reported by Lucenti et al.^{60,61} The authors investigated two “cyclic triimidazole” derivatives, namely triimidazo[1,2-a:1,2-c:1,2-e][1,3,5]-triazine (**39**) and benzo[4,5]imidazo[1,2]benzo[4,5]imidazo-[1,2-c]benzo[4,5]imidazo[1,2-e][1,3,5]triazine (**40**). In solution at RT both compounds display only fluorescent emission with Φ increasing from **39** (2%) to **40** (17%). Noticeably, based on TDDFT calculations, emission of **40** was associated to deactivation from an S_2 excited state in agreement with the zero oscillator strength of its S_0 - S_1 transition. On the other side, crystals of **39** show a strong, broad, featureless emission centered at 425 nm ($\Phi = 30\%$) which is the result of the superimposition of a prompt ($\lambda_{em} = 400$ nm, τ in the nanosecond regime) and a longer wavelength ($\lambda_{em} = 520$ nm) ultralong delayed component which lasts for about 3.6 s (τ up to 990 ms) and is affected by the degree of crystallinity but inert to oxygen, as indicated by the time-resolved emission experiments performed by the authors. Single crystal XRD analysis revealed that the molecules are arranged in H aggregates through face to face strong π - π interactions (distances between centroids of the central rings equal to 3.95 and 3.73 Å) (see Figure 19). The role of such aggregates in the RTUP of **39** was supported by the photophysical behavior of its isomer **39-a** lacking H aggregates in its crystal structure. **39-a** displays CIE behavior, being very poorly emissive in solution ($\Phi = 2.8\%$) but quite so in crystals ($\lambda_{em} = 415$ nm, $\Phi = 13\%$), but with fast emission decay (in the ns regime) even at 77 K. Intriguingly, solid **40** shows at RT both phosphorescence and dual fluorescence (with an overall Φ equal to 18%) which can be selectively activated by varying the excitation wavelength. At 260 nm, a near-UV fluorescence emission ($\lambda_{em} = 350$ nm, τ nanosecond regime) of S_2 - S_0 origin, similar to that of the chromophore in dilute solution, is observed. By exciting at 370 nm a structured blue fluorescence ($\lambda_{em} = 407$ nm, τ in the ns regime) superimposed onto a RTUP ($\lambda_{em} = 530$ nm, τ up to 0.5 s) is produced resulting in white light emission. The presence of this second fluorescence of S_1 - S_0 nature, selectively activated only by populating the S_1 state, was explained by the authors,

by partial loss of the molecular symmetry of the chromophore owing to interchromophoric interactions in the solid state. Due to the impossibility of obtaining single crystals of **40** suitable for XRD analysis, the presence of H aggregates was guessed based on the similarity of its RTUP emission with that of **39**.

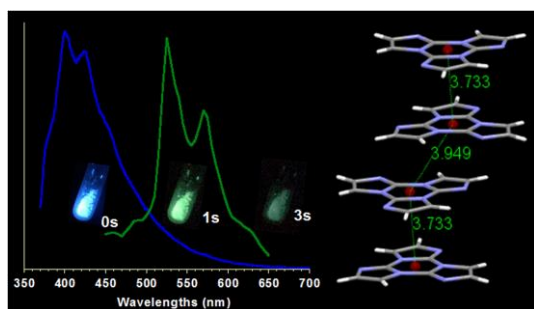


Figure 19. Left: Photoluminescence (blue line, $\lambda_{\text{exc}} = 350$ nm) and phosphorescence (green line, time delay = 472 ms, $\lambda_{\text{exc}} = 374$ nm) of crystals of **39** at 298 K. Inset: photographs of the crystals taken under excitation at 365 nm (0 s) and after excitation was turned off (1 and 3 s); Right: fragment of crystal packing of **39** showing distances between centroids of overlapped triazinic rings (red circles). (Reprinted with permission from ref. 62. Copyright 2017, American Chemical Society).

Further evidence of the role of strong π - π stacking interactions in the phosphorescence properties of purely organic materials was provided by Yong et al.,⁶² who investigated the emissive behavior of a carboxylic acid radical, namely 2-(imidazo[1,2-a]pyridin-2-yl)-2-oxoacetic acid (**41**), and its sodium salt (**41-a**). H_2O and DMSO solutions of these compounds display quite similar RTP in the UV region (360–380 nm, $\tau = 16.7$ – 28.3 μs), due to either the presence of the aromatic carbonyl group which favors triplet generation through ISC or the free single-electron which is present in these radicalic species. A different emissive behavior is instead observed in the solid state: **41** exhibits white-light RTP (from 395 to 750 nm, maximum at 483 nm, $\tau = 19.4$ μs , $\Phi = 5.2$ %), a rare case of single-component organic phosphorescent material with such emission feature, while **41-a** displays blue-light RTP ($\lambda_{\text{em}} = 441$ nm, $\tau = 22.8$ μs , $\Phi_{\text{p}} = 7.5$ %). In both cases, the band position does not change with excitation wavelength λ_{exc} (only their intensity increases with increasing λ_{exc}), implying that the nature of the emission remains unvaried. According to the authors, the broad emission band observed for **41** originates from both molecular and aggregate contributions. In fact, single crystal XRD analysis of **41**· H_2O revealed that its crystal structure consists of one-dimensional columnar stacking chains laterally connected through bridging water molecules forming infinite planes. Within the stack, C \cdots C intermolecular contacts shorter than the sum of the van der Waals radii indicate effective intermolecular orbital overlap. Looking at the short distances both between planes of the aromatic fused rings and their centroids along the stack (alternately equal to 3.114, 3.382 Å and 4.996, 3.853 Å, respectively), denoting slightly slipped stacking mode, we suggest the presence of H-aggregation in the crystal structure of **41**· H_2O (see Figure 20). In view of the recent literature in this regard, we propose that the lack of the expected RTUP could be motivated by the presence

of water in the crystal structure, which is well known to strongly contribute to nonradiative deactivation through OH vibrations. The change in emission color displayed by the solid-state sodium salt, **41-a**, was ascribed to a packing mode different from that of **41**, though no information in this regard can be given owing to the lack of single crystal data.

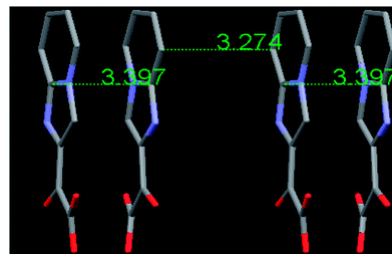
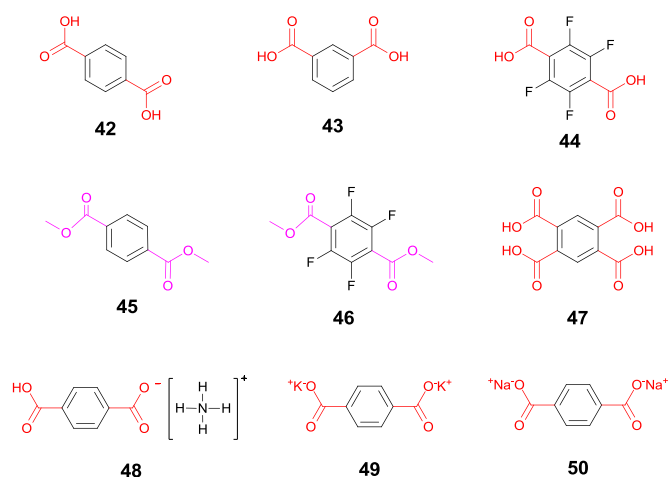


Figure 20. The columnar stacking chain in **41**· H_2O . (Adapted from ref. 62 with permission from The Royal Society of Chemistry).

Table 6 RTP Emission Maxima (λ_{em}) and Lifetimes (τ) of compounds **38-41**

Compound		Phosphorescence			Reference
Label	Structure	λ_{em} (nm)	Φ_P (%)	τ (ms)	
38a		544	4.0	79.8	58
38b		588		61.8	
38c		540	4.4	18.6	
39		525 570		990	60
40		530		515	61
41		483	5.2	19.4×10^{-3}	62
41-a		441	7.5	22.8×10^{-3}	62

**Chart 9.** Terephthalic derivatives **42-50**.

An example of the difficulty in the interpretation of compounds' photophysical behavior is provided by the different studies appeared on terephthalic acid (**42**) and its derivatives.

In 2015 Gong et al.⁶³ reported on the photoluminescence of **42**, isophthalic acid (**43**), tetrafluoroterephthalic acid (**44**) and their relative esters (**45** and **46**). All these compounds are almost non emissive in solution and in disordered amorphous states due to vibrational and rotational dissipations (as confirmed also by the presence of afterglow for **42** in ethanol solution at 77 K) (see Figure 21). However, crystalline powders of the compounds display intensified emission (with overall Φ from 1.5% for **45** to 15.3% for **43**) by concomitant prompt fluorescence (nanosecond regime), delayed fluorescence and phosphorescence (τ from 2.69 ms for **45** to 289.96 ms for **43**) at RT.

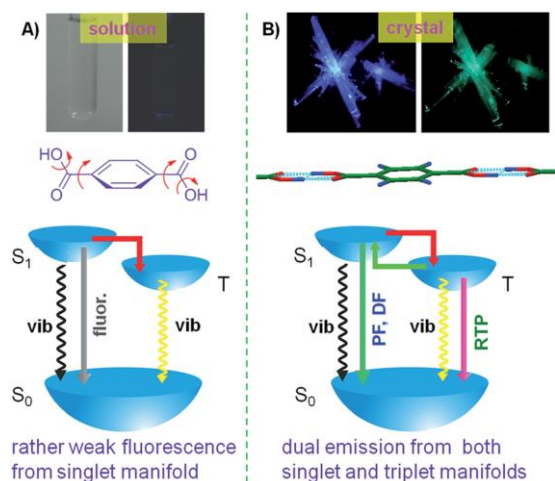


Figure 21. Schematic illustration of the crystallization-induced dual emission phenomenon of **42**: (A) in solutions highly active molecular motions induce weak fluorescence and (B) in crystals conformation rigidification boost both prompt and delayed fluorescence, and phosphorescence. (Adapted from ref. 63 with permission from The Royal Society of Chemistry).

By a careful analysis of their crystal structures, the authors attributed the CIE behavior of these compounds to the presence of abundant intermolecular short contacts which rigidify the molecular conformations and prevent dissipation through molecular motions. Moreover, TDDFT calculations indicated reduced energy gap and enhanced SOC between the triplet and singlet states involved in the emission in the crystalline state. In addition, the solid state red-shifted fluorescence (up to 75 nm) of the acids with respect to their solution, was attributed to the formation of dimeric units with an extended planar skeleton by intermolecular hydrogen bonds. The intermolecular electronic communication of these dimers is absent in the relative esters, due to the lack of the dimeric stacking.

In a parallel study performed by Kuno et al.,⁶⁴ the presence of closely packed dimeric units in the crystal lattice of **43** and other benzoic acids (**42** and pyromellitic acid, **47**) was indicated as crucial to observe RTP. Through a detailed investigation, the authors proposed that the triplet state T₁ responsible for the phosphorescent emission is populated by hyperfine coupling (HFC) mechanism mediated by the local magnetic field of neighbouring ¹H nuclear spins. In such case ISC is realized by a singlet to triplet conversion of weakly bound radical ion pairs (RIP) generated by photoexcitation of the CT complex formed by two molecules packed with a π-π distance below 4 Å (in this case 3.76 Å). The presence of singlet and triplet RIPs was confirmed by the observation that an external magnetic field affects the phosphorescent emission. In particular, low magnetic fields decrease the emission intensity due to HFC suppression by the Zeeman splitting of three degenerate triplet states, while an increased phosphorescence is observed at high fields as a result of the spin exchanges enhancement. Further evidences on the involvement of ¹H nuclear spins were provided by a C-deuterated derivative of **43** showing a reduction of the phosphorescence intensity. This behavior was explained in terms of a lower HFC constant for the D nuclear spin, causing a

retarded singlet to triplet conversions in RIPs, while a common S₁-T₁ ISC pathway should benefit by deuteration that reduces non-radiative relaxations. This was in fact observed when deuterium substitution was performed on the hydroxylic groups of **43** where a slight increase of the phosphorescent emission was observed due to minor O-H vibrations quenching.

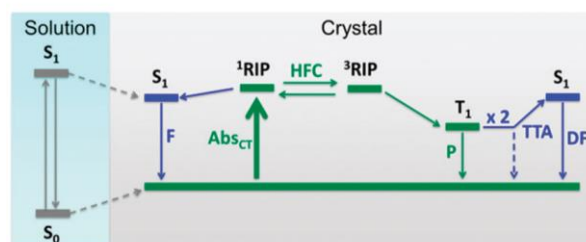
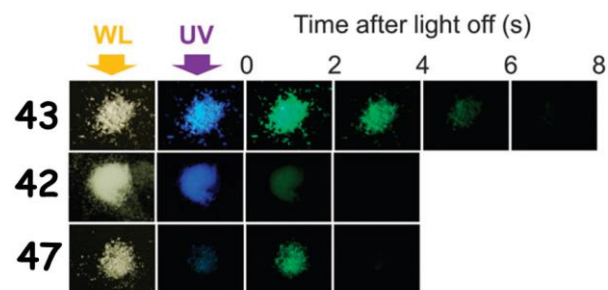


Figure 22. Top: afterglows of crystalline **43**, **42**, and **47**. Bottom: State energy diagram for **43** phosphorescence. Green color shows the route to phosphorescence emission and blue color shows the route to fluorescence and delayed fluorescence. Abs_{CT}: CT absorption, P: Phosphorescence, TTA: triplet-triplet annihilation, DF: delayed fluorescence, HFC: hyperfine coupling. (Adapted from ref. 64 with permission from The Royal Society of Chemistry).

The overall mechanism can be summarized as follow: closely packed **43** molecules in the solid state generate a CT complex that gives ¹RIP by photoexcitation. By HFC ¹RIP easily exchange with ³RIP that produces a T₁ state responsible of the phosphorescence. The involvement of the T₁ state rather than ³RIP in the RTP is supported by the large Stokes shift, by lifetime reduction in halo-substituted derivatives and by observation of delayed fluorescence by TTA mechanism (see Figure 22).

In 2018 Cheng et al.⁶⁵ reported the first example of RTUP in ionic organic crystals based on **42**, namely ammonium hydrogen terephthalate (**48**), dipotassium terephthalate (**49**) and disodium terephthalate (**50**). The photophysical characterization of the three crystalline compounds under ambient conditions revealed the presence of both fluorescence and ultralong phosphorescence, this latter with colour changing from green for **48** (λ_{em} = 502 nm, τ = 586 ms) and **50** (λ_{em} = 508 nm, τ = 585 ms) to blue for **49** (λ_{em} = 456 nm, τ = 504 ms). Single crystal XRD analysis of **48** indicated a larger torsion angle between the carbonyl group and benzene ring with respect to **42**. This structural feature has been suggested by the authors to favor ISC to triplet states. Furthermore, the presence of face-to-face stacking (interplanar distance equal to 3.510 Å) with formation of H aggregates was assumed to be responsible for the RTUP (see Figure 23), that is enhanced by restricted molecular motions caused by the multiple intermolecular

interactions in the crystal and by ionic bonding between the ammonium and terephthalate ions. Similar features were identified also in the other two crystalline compounds. In particular, a reduction of the π - π distance on going from **49** (3.571 Å) to **50** (3.268 Å) was associated with more stable H aggregates and longer RTP emission.

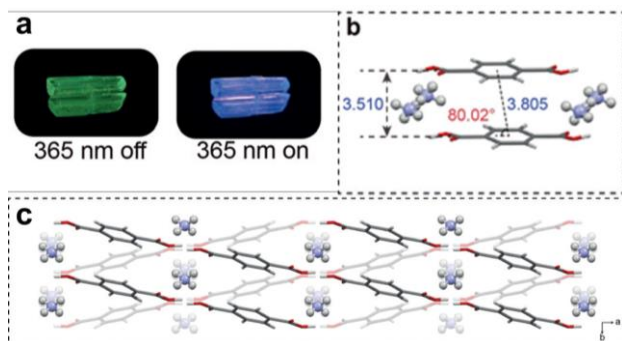


Figure 23. a) Photographs of **48** crystal before and after irradiation with a 365 nm UV lamp. b) Molecular packing in dimer with the distance between intermolecular planes or centers highlighted in blue; c) Intermolecular stacking viewed along the c axis. (Adapted with permission from ref. 65. Copyright 2018, Wiley-VCH Verlag GmbH & Co. KGaA).

Boron-containing compounds are known to be very sensitive to intramolecular motions and collisions with quenching species, however many boronic derivatives have been found to display RTUP properties in the crystalline state thanks to various suggested mechanisms.

In 2017 Kuno and coworkers,⁶⁶ following their earlier report,⁶⁴ explained the RTUP of crystalline derivatives of the phenylboronic acid through ISC accomplished by HFC mechanism. In particular, phenyl-mono-boronic acid (**51**), 1,4-phenylenediboronic acid (**52**) and p-phenylenediboronic acid ethyleneglycol ester (**53**) display delayed fluorescence ($\lambda_{em} = 322$ nm, $\tau = 0.49$ s; $\lambda_{em} = 329$ nm, $\tau = 0.35$ s and $\lambda_{em} = 331$ nm, $\tau = 0.55$ s for **51**, **52** and **53** respectively) and RTUP with “afterglow” lifetime increasing in the order **51**<**52**<**53** ($\lambda_{em} = 482$ nm, $\tau = 1.2$ s; $\lambda_{em} = 494$ nm, $\tau = 0.95$ s and $\lambda_{em} = 503$ nm, $\tau = 1.6$ s with overall quantum efficiency equal to 18, 66, 77 for **51**, **52** and **53** respectively) (see Figure 24).

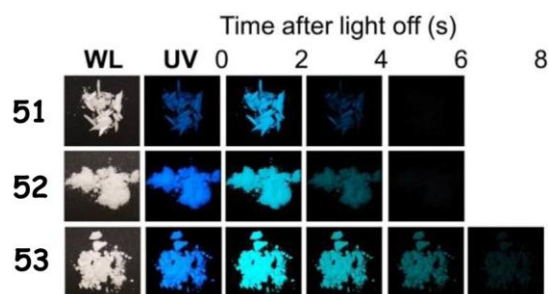


Figure 24. “Afterglows” of crystalline **51**, **52** and **53** after irradiation with a hand-held lamp at 254 nm. WL=under white light; UV=under UV light. The lifetimes of the afterglows visually appeared to be about twice as long as those obtained with CCD camera images. (Adapted with permission from ref. 66. Copyright 2017, Wiley-VCH Verlag GmbH & Co. KGaA).

Table 8 RTP Emission Maxima (λ_{em}), Phosphorescence Quantum Efficiency (Φ_p), and Lifetimes (τ) of compounds **42-50**

Label	Compound	Phosphorescence		Reference
		λ_{em} (nm)	τ (ms)	
42		511	n.d.	63
		516	410	64
43		506	290	63
		468, 494, 532	970	64
44		484	18	63
45		446	2.69	63
46		492	9.12	63
47		533	1100	64
48		502	586	65
49		456	504	65
50		508	585	65

As in the previously reported example **43**, the present compounds showed phosphorescence dependence on magnetic-field and deuterium substitution, with no increase of phosphorescence intensity by heavy-atom effect but just a shortening of lifetimes in halogen substituted derivatives. TDDFT calculations on **52** revealed that the CT complex was not formed by dimeric units which are arranged in head-to-tail manner but it is rather due to the presence of trimers. The authors also investigated the effect of increasing steric bulkiness in **52** esters with 1,2-propanediol, 2,3-butanediol and pinacol. As expected the bulkier substituents loose the molecular packing in crystal lattice, giving less efficient intermolecular electronic interactions or inhibiting formation of the CT complex resulting in reduced phosphorescent emission. In parallel, in 2017 Chai et al.⁶⁷ performed an investigation on the photophysical behavior of commercially available arylboronic acids (**54-62**) and their thermally prepared triphenylborazine derivatives (**t-54-t-62**) to support their idea that strong intermolecular interactions via hydrogen bonds may contribute to obtain a denser molecular packing thus favoring RTP, by partially suppressing the vibration in crystals and prolonging the triplet lifetime.

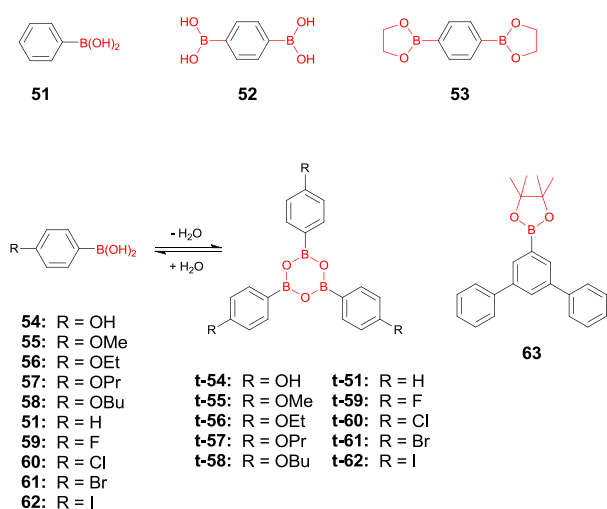


Chart 10. Phenylboronic acid derivatives **51-63**.

The authors observed that most of the analyzed compounds display solid state RTUP with lifetimes longer than 100 ms, the longest being observed for (4-methoxyphenyl)boronic acid (**55**) which was chosen as the representative. Solid **55** displays bright broad fluorescence ($\lambda_{em} = 302, 310-430$ nm, τ in the ns regime). However, after removal of the ultraviolet source, the emission changes from deep sky blue to cyan and slowly fades. The phosphorescence spectrum revealed the presence of two resolved emission peaks at 457 and 488 nm ($\tau = 2.24$ s and 2.19 s, respectively) which were unaffected by the presence of oxygen. In solution at RT, **55** doesn't display any phosphorescence neither in the absence nor in the presence of oxygen. However, in 77 K frozen solution, phosphorescence is turned on with blue-shifting and longer lifetimes upon increasing concentrations. Due to the similarity of phosphorescence maximum and lifetime of the diluted frozen solution and the crystals, the authors performed an investigation of the photophysical behavior of PMMA embedded thin film to establish the role of aggregation conformations and of the single molecules on crystalline RTP. It was observed that phosphorescence is present already at very low chromophore loading (0.01 wt%) and that, upon increasing the **55** content, a new red shifted fluorescence appears and the phosphorescent emission is red-shifted and stabilized (longer lifetime) becoming similar to that of the crystalline state. Based on this observation and by the lifetime prolonging in both PMMA and frozen solution at increasing concentration, it was guessed that the aggregation conformations determine the RTUP of the crystals and stabilize the triplet excitons. Single crystal XRD analysis of **55** and the other RTUP arylboronic acids, allowed to establish a relationship between the packing arrangement mode and RTUP properties indicating that both the rigid conformation which decreases the K_{nr} and the effective $\pi-\pi$ stacking which stabilizes the triplet states, contribute to the bright and persistent RTP. The importance of $\pi-\pi$ stacking interactions was further supported by TDDFT calculations on **55** monomers and dimers indicating that strong $\pi-\pi$ stacking decreases the singlet excited state energy and ΔE_{ST} , thereby

favoring ISC. Moreover, the effective overlap of orbitals increases the electronic delocalization stabilizing the triplet excitons and therefore increasing the RTP lifetime. In agreement, stronger $\pi-\pi$ stacking interactions brought to red-shifted emissions and longer RTUP lifetimes in **55**, **56** and **58**, compared to those of **54** and **57**.

In 2017 Yang et al.⁶⁸ reported on a new chromophore, namely 2-([1,1':3',1''-terphenyl]-5'-yl)-4,4,5,5-tetramethyl-1,3,2-dioxaborolane (**63**), which displays at RT a fluorescent emission at 350 nm with increasing quantum yields (from 5.4% to 28.9%) and lifetimes (from 5.2 to 12.1 ns) going from solution to the solid state, revealing its AIE character. At 77 K, the fluorescent emission is still present together with a phosphorescent emission ($\lambda_{em} = 450$ nm, $\tau = 5.5$ and 2.2 s for solution and powders, respectively) (see Figure 25). Interestingly, the same dual fluorescence/phosphorescence emission is observed in solid samples at RT after mechanical grinding. Single crystal XRD analysis indicated the absence of $\pi-\pi$ stacking but the presence of several intra- and inter-molecular interactions. In particular, two types of coupled **63** molecules were identified: a strongly coupled (characterized by intermolecular C-H...O distance of 3.184 Å) and a weakly coupled one with intermolecular C-H...O distance of 3.540 Å. The strong interactions of oxygen atoms with phenyl rings of adjacent molecules were accountable to favour the $n-\pi^*$ transition and enhance ISC crossing, and also to reduce non-radiative relaxations and increase phosphorescent efficiency. These results were supported by TDDFT calculations performed on monomeric and dimeric **63**, as derived from the single-crystal structure, which revealed the presence of four main ISC transitions from S_1 to T_n in the case of the strongly coupled **63** and only one possible ISC transition in the weakly coupled molecules. Based on these observations, the authors explained the mechanophosphorescence of the compound as due to the increased coupling degree of two **63** molecules by sample grinding. In addition, the mechanical stimulation was suggested to have a positive effect on the relative location of the excited states favoring ISC transitions which are otherwise difficult at RT being all S_1-T_n transitions endothermic, in agreement with the absence of phosphorescence from the unground powders. In agreement with the crucial role of intra- and intermolecular interactions in the mechanoluminescent behaviour of **63**, no phosphorescence and remarkably reduced fluorescent emission was observed in an amorphous sample obtained by vigorous grinding.

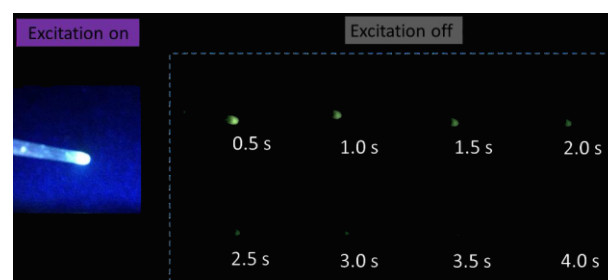


Figure 25. UP pictures of **63** solid taken at different times before and after turn-off of the excitation (254 nm) at 77K. (Reprinted with permission from ref. 68. Copyright 2017, Wiley-VCH Verlag GmbH & Co. KGaA).

Table 9 RTP Emission Maxima (λ_{em}) and Lifetimes (τ) for compounds **51-63**

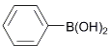
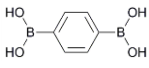
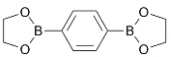
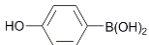
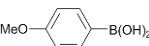
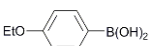
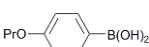
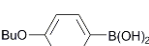
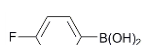
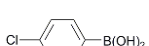
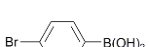
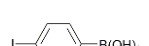
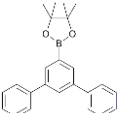
Compound		Phosphorescence		Reference
Label	Structure	λ_{em} (nm)	τ (ms)	
51		482	1200	66
		493	890	67
52		494	950	66
53		503	1600	66
54		491	710	67
55		457	2190	67
		488	2240	
56		488	1110	67
57		506	130	67
58		492	1280	67
59		492	1340	67
60		593	370	67
61		546	73	67
62		540	n.d.	67
63-ground		450	n.d.	68


Table 10 RTP Emission Maxima (λ_{em}) and Lifetimes (τ) for compounds **t-51-t-62**

Compound			Phosphorescence		Reference
Label	Structure		λ_{em} (nm)	τ (ms)	
t-51	R = H		494	160	67
t-54	R = OH		486	580	67
t-55	R = OMe		503	710	67
t-56	R = OEt		500	n.d.	67
t-57	R = OPr		492	n.d.	67
t-58	R = OBu		444	n.d.	67
t-59	R = F		500	1960	67
t-60	R = Cl		512	250	67
t-61	R = Br		480	170	67
t-62	R = I		520	n.d.	67

RTP from concomitant XB and π - π interactions

Some solid compounds may display a multifaceted phosphorescent behavior associated with different interchromophoric interactions concomitantly present in the aggregated phase. Such emissions possess different properties and can be selectively activated in different conditions.

A comprehensive example of multiple interactions which coexist in the solid state producing different RTP emissions has been provided by Lucenti et al.⁶¹ for 3,7-dibromotriimidazo[1,2-a:1',2'-c:1'',2''-e][1,3,5]triazine (**64**), the dibromo derivative of cyclic triimidazole **39** above discussed. While DCM solutions of **64** at RT display only hardly discernible fluorescent emission (λ_{em} = 380 nm), at 77 K the emission spectrum is dominated by an intense phosphorescent band (λ_{em} = 580 nm, τ = 265 μ s), excited only at wavelengths below 280 nm and unaffected by the presence/absence of oxygen. On the basis of DFT/TDDFT calculations, this emission has been ascribed to the presence of

a T_n level with $\sigma \rightarrow \sigma^*$ symmetry, where the σ orbital is mainly localized on the bromine atom, which allows efficient ISC from the closest S_n levels. IC to T_1 then leads to the observed molecular phosphorescence. Powders of **63** show at RT a structured fluorescence (λ_{em} = 395, 419 and 443 nm, τ = 0.71 ns), a broad short-lived (λ_{em} = 470 nm, τ = 1.25 ms) and a structured long-lived phosphorescence (λ_{em} = 553, 600 nm, τ = 49 ms), with an overall quantum efficiency of 14%. Moreover, the relative intensity of the long-lived component increases with increasing crystallinity of the sample, while that of the short-lived one is rather insensitive to the crystallinity. In fact, thin films with relatively high concentrations of **64** in PMMA (10%w/w) revealed at RT the presence of the 470 nm short-lived phosphorescence, though only in the absence of oxygen. Single crystal XRD analysis showed that the crystal structure consists of slightly corrugated planes of almost overlapped molecules, forming H-aggregates through strong π - π interactions (distances between centroids of the triazine rings equal to 4.068 Å) (see Figure 26). Similar to **39**, such aggregates

are deemed to be responsible for the long-lived RTP. Moreover, within the planes, adjacent molecules are arranged in tetrameric Br...Br XB cyclic units (Br₄ synthons)⁶⁹ with Br...Br distances of 3.596 and 3.608 Å.

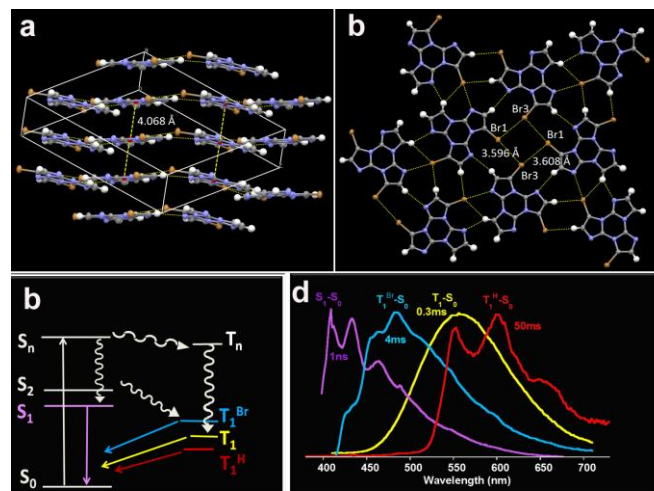


Figure 26. a) Crystal packing of **64** showing the parallel arrangement of the layers (distance between triazine centroids highlighted by yellow line); b) View down the *a* direction showing the Br...Br XB pattern; c) Schematic representation of the main photophysical processes of **64**; d) fluorescent and phosphorescent emissions of solid **64** with RTUP in red.

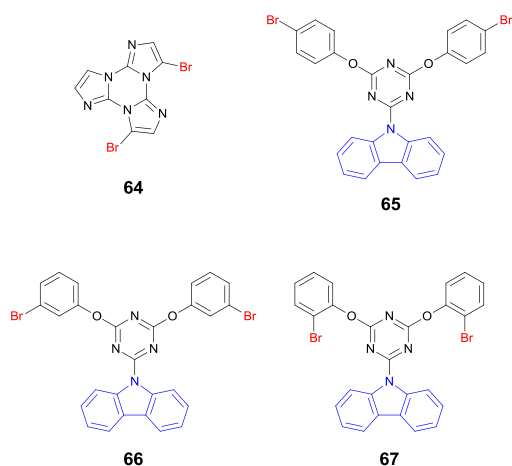


Chart 11. Compounds with concomitant XB and π - π interactions **64-67**.

The Br₄ synthon shows a “type II” geometrical disposition, with the positive σ -hole located on each halogen X along the extension of the C–X bond and points towards the negative belt around the adjacent X atom. Such Br...Br tetrameric aggregate generates the RTP observed at about 470 nm. Interestingly, the corresponding mono-substituted derivative, where neither H-aggregates nor Br...Br XBs are present in the crystal structure, does not show any phosphorescent emission at RT, while only the molecular phosphorescence at 580 nm, due to bromine atom, is observed at low temperature.

The synergistic effect of H aggregates and XB has also been considered responsible of the RTUP behavior of three isomeric Cz-triazine derivatives reported very recently by Cai et al.,⁷⁰ namely 9-(4,6-bis(4-bromophenoxy)-1,3,5-triazin-2-yl)-9H-carbazole (**65**), 9-(4,6-bis(3-bromophenoxy)-1,3,5-triazin-2-yl)-9H-carbazole (**66**), and 9-(4,6-bis(2-bromophenoxy)-1,3,5-triazin-2-yl)-9H-carbazole (**67**). In the dilute THF solution, the three derivatives display at RT an identical broad fluorescence ($\lambda_{em} = 450$ nm) of ICT character and at 77 K the same fluorescence (main peak at $\lambda_{em} = 338$ nm) and phosphorescence ($\lambda_{em} = 400$ –50 nm) indicating no impact of the Br-substitution position on the molecular luminescence. In the crystal state, the three compounds show both intense fluorescence ($\lambda_{em} = 370$ –400 nm, τ in the nanosecond region, $\Phi = 10$, 3 and 47 % for **65**, **66**, and **67** respectively) and oxygen-insensitive phosphorescence ($\lambda_{em} = 530$ –634 nm, $\tau = 155$, 120, 156 ms for **65**, **66**, and **67** respectively) with quantum yield increasing in the order **67**, **65**, **66** ($\Phi_p = 2.3$, 8, 13% respectively). The photophysical behavior of the three compounds was interpreted by the authors by means of theoretical calculation and single crystal XRD analysis. TDDFT calculations revealed an increased number of transition channels for ISC for dimers of **65** with respect to the monomer, while no increase was calculated for dimers of **66** and **67** with respect to the corresponding monomers. From single crystal XRD analysis, H aggregates are evident in the crystal structure of all three isomers indicating their role in the stabilization of the triplet excited states for RTUP. In addition, while C–Br...H–C distance is the same in the three compounds, the C–Br... π one is much shorter for **66** (3.461 Å) than for **65** (3.759 Å) and **67** (3.805 Å). According to the authors, this short distance together with a favorable C–Br... π angle, α (equal to 116.7°, see Figure 27) in **66** facilitate SOC for high efficient RTUP.

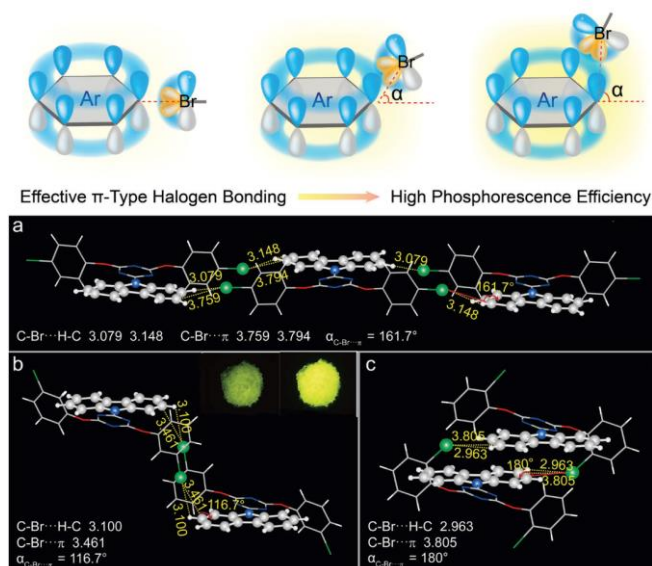
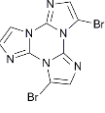
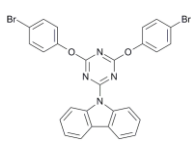
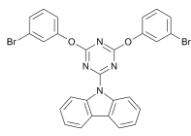
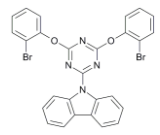


Figure 27. Top: Schematic illustration of three types of C–Br... π XB. Bottom: Intermolecular interactions in a) **65**, b) **66**, and c) **67** crystal. Inset: photographs of crystalline powder of **66** under 365 nm lamp on (left) and off (right). (Adapted with permission from ref. 70. Copyright 2018, Wiley-VCH Verlag GmbH & Co. KGaA).

Table 11 RTP Emission Maxima (λ_{em}), Phosphorescence Quantum Efficiency (Φ_p) and Lifetimes (τ) for compounds **64-67**

Compound		Phosphorescence			Reference
Label	Structure	λ_{em} (nm)	Φ_p (%)	τ (ms)	
64		470 553, 600		1.25 49	61
65		539 581 634	7.7	155 154 154	70
66		530 572 622	13	109 120 68	70
67		532 573 624	2.3	156 158 157	70

Conclusions

Through an extensive series of examples appeared in the literature, the fundamental role of interchromophoric interactions in activating or affecting the phosphorescent behaviour of organic aggregated samples is clearly demonstrated. We have focused our attention on XB and π - π interactions, mentioning other suggested mechanisms when referred to the same class of molecules. Such mechanisms may of course act in a synergic way, one not excluding the others. The role of the crystal phase in the examples reported goes beyond that of rigidification and protection of the luminophor, which is of course always to be considered.

The large number of papers appeared in the last 3-4 years clearly indicates the newly born and growing interest in self-interaction induced organic RTP.

Conflicts of interest

There are no conflicts to declare.

References

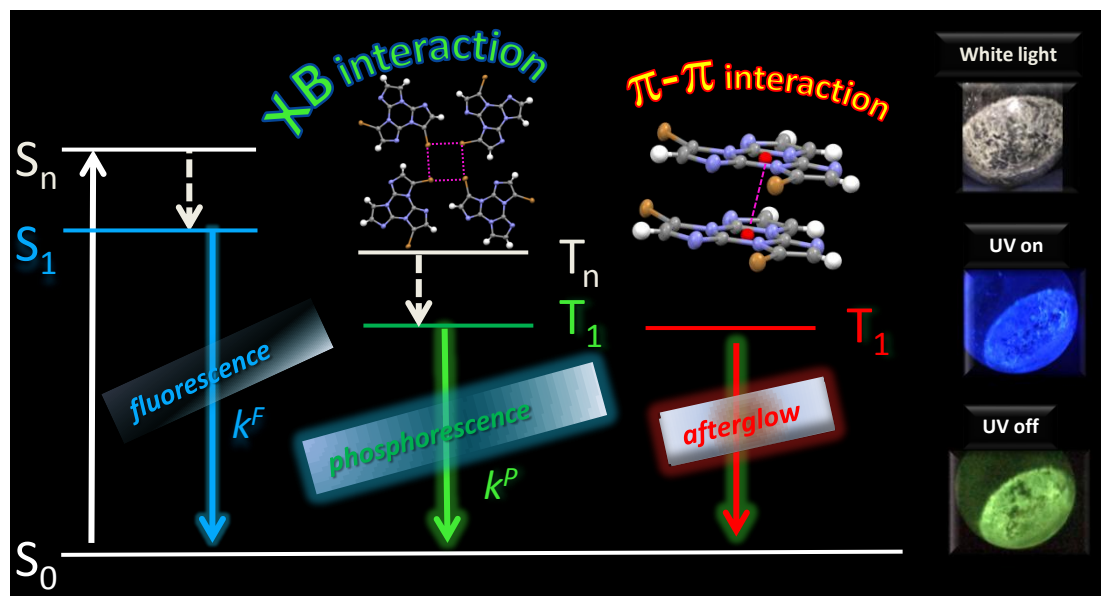
- 1 L. Ravotto and P. Ceroni, *Coord. Chem. Rev.*, 2017, **346**, 62-76.
- 2 C. S. Bilen, N. Harrison and D. J. Morantz, *Nature*, 1978, **271**, 235.
- 3 S. Hirata, *Adv. Opt. Mater.*, 2017, **5**, 1700116.
- 4 H. L. Chen, Y. F. Huang, T. S. Lim, C. H. Su, P. H. Chen, A. C. Su, K. T. Wong, T. C. Chao, S. I. Chan and W. Fann, *J. Phys. Chem. B*, 2009, **113**, 8527-8531.
- 5 M. A. El-Bayoumi and F. M. A. Halim, *J. Chem. Phys.*, 1968, **48**, 2536-2541.
- 6 T. Benincori, G. Bongiovanni, C. Botta, G. Cerullo, G. Lanzani, A. Mura, L. Rossi, F. Sannicolò and R. Tubino, *Phys. Rev. B*, 1998, **58**, 9082-9086.
- 7 Y. Ren, J. W. Y. Lam, Y. Dong, B. Z. Tang and K. S. Wong, *J. Phys. Chem. B*, 2005, **109**, 1135-1140.
- 8 T. Virgili, A. Forni, E. Cariati, D. Pasini and C. Botta, *J. Phys. Chem. C*, 2013, **117**, 27161-27166.
- 9 M. M. Mroz, S. Benedini, A. Forni, C. Botta, D. Pasini, E. Cariati and T. Virgili, *PCCP*, 2016, **18**, 18289-18296.
- 10 E. Cariati, V. Lanzeni, E. Tordin, R. Ugo, C. Botta, A. Giacometti Schieronni, A. Sironi and D. Pasini, *PCCP*, 2011, **13**, 18005-18014.
- 11 Y. Dong, J. W. Y. Lam, A. Qin, J. Sun, J. Liu, Z. Li, J. Sun, H. H. Y. Sung, I. D. Williams, H. S. Kwok and B. Z. Tang, *Chem. Commun.*, 2007, 3255-3257.

- 12 Z. Li, Y. Q. Dong, J. W. Y. Lam, J. Sun, A. Qin, M. Häußler, Y. P. Dong, H. H. Y. Sung, I. D. Williams, H. S. Kwok and B. Z. Tang, *Adv. Funct. Mater.*, 2009, **19**, 905-917.
- 13 W. Z. Yuan, X. Y. Shen, H. Zhao, J. W. Y. Lam, L. Tang, P. Lu, C. Wang, Y. Liu, Z. Wang, Q. Zheng, J. Z. Sun, Y. Ma and B. Z. Tang, *J. Phys. Chem. C*, 2010, **114**, 6090-6099.
- 14 Y. Li, M. Gecevicius and J. Qiu, *Chem. Soc. Rev.*, 2016, **45**, 2090-2136.
- 15 Y. Yang, K.-Z. Wang and D. Yan, *ACS Appl. Mater. Interfaces*, 2016, **8**, 15489-15496.
- 16 S. Mukherjee and P. Thilagar, *Chem. Commun.*, 2015, **51**, 10988-11003.
- 17 J. Yuan, Y. Tang, S. Xu, R. Chen and W. Huang, *Science Bulletin*, 2015, **60**, 1631-1637.
- 18 C.-R. Wang, Y.-Y. Gong, W.-Z. Yuan and Y.-M. Zhang, *Chin. Chem. Lett.*, 2016, **27**, 1184-1192.
- 19 S. Wang, W. Z. Yuan and Y. Zhang, in *Aggregation-Induced Emission: Materials and Applications Volume 2*, American Chemical Society, 2016, vol. 1227, ch. 1, pp. 1-26.
- 20 Y. Liu, G. Zhan, Z.-W. Liu, Z.-Q. Bian and C.-H. Huang, *Chin. Chem. Lett.*, 2016, **27**, 1231-1240.
- 21 S. Xu, R. Chen, C. Zheng and W. Huang, *Adv. Mater.*, 2016, **28**, 9920-9940.
- 22 S. Wu, Z. Pan, R. Chen and X. Liu, in *Long Afterglow Phosphorescent Materials*, eds. S. Wu, Z. Pan, R. Chen and X. Liu, Springer International Publishing, Cham, 2017, pp. 117-151.
- 23 M. Baroncini, G. Bergamini and P. Ceroni, *Chem. Commun.*, 2017, **53**, 2081-2093.
- 24 C. Li, X. Tang, L. Zhang, C. Li, Z. Liu, Z. Bo, Y. Q. Dong, Y.-H. Tian, Y. Dong and B. Z. Tang, *Adv. Opt. Mater.*, 2015, **3**, 1184-1190.
- 25 X. Pang and W. J. Jin, in *Halogen Bonding II. Topics in Current Chemistry*, eds. P. Metrangolo and G. Resnati, Springer International Publishing, Cham, 2014, vol. 359, pp. 115-146.
- 26 M. Shimizu, A. Kimura and H. Sakaguchi, *Eur. J. Org. Chem.*, 2016, **2016**, 467-473.
- 27 M. Shimizu, R. Shigitani, M. Nakatani, K. Kuwabara, Y. Miyake, K. Tajima, H. Sakai and T. Hasobe, *J. Phys. Chem. C*, 2016, **120**, 11631-11639.
- 28 J. Yang, Z. Ren, B. Chen, M. Fang, Z. Zhao, B. Z. Tang, Q. Peng and Z. Li, *J. Mater. Chem. C*, 2017, **5**, 9242-9246.
- 29 M. Baba, *J. Phys. Chem A*, 2011, **115**, 9514-9519.
- 30 J. Zhao, W. Wu, J. Sun and S. Guo, *Chem. Soc. Rev.*, 2013, **42**, 5323-5351.
- 31 M. A. El-Sayed, *Acc. Chem. Res.*, 1968, **1**, 8-16.
- 32 S. Hirata, K. Totani, J. Zhang, T. Yamashita, H. Kaji, S. R. Marder, T. Watanabe and C. Adachi, *Adv. Funct. Mater.*, 2013, **23**, 3386-3397.
- 33 S. Reineke and M. A. Baldo, *Sci. Rep.*, 2014, **4**, 3797.
- 34 O. Bolton, K. Lee, H.-J. Kim, K. Y. Lin and J. Kim, *Nat. Chem.*, 2011, **3**, 205-210.
- 35 H. Shi, Z. An, P.-Z. Li, J. Yin, G. Xing, T. He, H. Chen, J. Wang, H. Sun, W. Huang and Y. Zhao, *Cryst. Growth Des.*, 2016, **16**, 808-813.
- 36 S. K. Maity, S. Bera, A. Paikar, A. Pramanik and D. Haldar, *Chem. Commun.*, 2013, **49**, 9051-9053.
- 37 R. Bosisio, C. Botta, A. Colombo, S. Destri, W. Porzio, E. Grilli, R. Tubino, G. Bongiovanni, A. Mura and G. Di Silvestro, *Synth. Met.*, 1997, **87**, 23-29.
- 38 J. Cornil, D. A. dos Santos, X. Crispin, R. Silbey and J. L. Brédas, *J. Am. Chem. Soc.*, 1998, **120**, 1289-1299.
- 39 E. G. McRae and M. Kasha, *J. Chem. Phys.*, 1958, **28**, 721-722.
- 40 M. Kasha, H. R. Rawls and M. Ashraf El-Bayoumi, *Pure Appl. Chem.*, 1965, **11**, 371-392.
- 41 G. S. Levinson, W. T. Simpson and W. Curtis, *J. Am. Chem. Soc.*, 1957, **79**, 4314-4320.
- 42 D. J. Morantz, C. S. Bilen and N. Harrison, *Polymer*, 1978, **19**, 473-474.
- 43 M. C. Castex, C. Olivero, G. Pichler, D. Ades and A. Siove, *Synth. Met.*, 2006, **156**, 699-704.
- 44 Z. Yang, Z. Mao, X. Zhang, D. Ou, Y. Mu, Y. Zhang, C. Zhao, S. Liu, Z. Chi, J. Xu, Y.-C. Wu, P.-Y. Lu, A. Lien and M. R. Bryce, *Angew. Chem. Int. Ed.*, 2016, **55**, 2181-2185.
- 45 S. Hirata and M. Vacha, *Adv. Opt. Mater.*, 2017, **5**, 1600996.
- 46 Y. Liu, G. Zhan, P. Fang, Z. Liu, Z. Bian and C. Huang, *J. Mater. Chem. C*, 2017, **5**, 12547-12552.
- 47 C. Sun, X. Ran, X. Wang, Z. Cheng, Q. Wu, S. Cai, L. Gu, N. Gan, H. Shi, Z. An, H. Shi and W. Huang, *J. Phys. Chem. Lett.*, 2018, **9**, 335-339.
- 48 Z. An, C. Zheng, Y. Tao, R. Chen, H. Shi, T. Chen, Z. Wang, H. Li, R. Deng, X. Liu and W. Huang, *Nat. Mater.*, 2015, **14**, 685-690.
- 49 X. Zhen, Y. Tao, Z. An, P. Chen, C. Xu, R. Chen, W. Huang and K. Pu, *Adv. Mater.*, 2017, **29**, 1606665.
- 50 L. Gu, H. Shi, C. Miao, Q. Wu, Z. Cheng, S. Cai, M. Gu, C. Ma, W. Yao, Y. Gao, Z. An and W. Huang, *J. Mater. Chem. C*, 2018, **6**, 226-233.
- 51 P. Xue, J. Sun, P. Chen, P. Wang, B. Yao, P. Gong, Z. Zhang and R. Lu, *Chem. Commun.*, 2015, **51**, 10381-10384.
- 52 S. Cai, H. Shi, J. Li, L. Gu, Y. Ni, Z. Cheng, S. Wang, W.-w. Xiong, L. Li, Z. An and W. Huang, *Adv. Mater.*, 2017, **29**, 1701244.
- 53 Y. Xie, Y. Ge, Q. Peng, C. Li, Q. Li and Z. Li, *Adv. Mater.*, 2017, **29**, 1606829.
- 54 Y. Gong, G. Chen, Q. Peng, W. Z. Yuan, Y. Xie, S. Li, Y. Zhang and B. Z. Tang, *Adv. Mater.*, 2015, **27**, 6195-6201.
- 55 S. M. A. Fateminia, Z. Mao, S. Xu, Z. Yang, Z. Chi and B. Liu, *Angew. Chem. Int. Ed.*, 2017, **56**, 12160-12164.
- 56 Z. Mao, Z. Yang, Y. Mu, Y. Zhang, Y.-F. Wang, Z. Chi, C.-C. Lo, S. Liu, A. Lien and J. Xu, *Angew. Chem. Int. Ed.*, 2015, **54**, 6270-6273.
- 57 Z. He, W. Zhao, J. W. Y. Lam, Q. Peng, H. Ma, G. Liang, Z. Shuai and B. Z. Tang, *Nat. Commun.*, 2017, **8**, 416.
- 58 S. Cai, H. Shi, Z. Zhang, X. Wang, H. Ma, N. Gan, Q. Wu, Z. Cheng, K. Ling, M. Gu, C. Ma, L. Gu, Z. An and W. Huang, *Angew. Chem. Int. Ed.*, 2018, Accepted Article.
- 59 T. Yu, D. Ou, Z. Yang, Q. Huang, Z. Mao, J. Chen, Y. Zhang, S. Liu, J. Xu, M. R. Bryce and Z. Chi, *Chem. Sci.*, 2017, **8**, 1163-1168.
- 60 E. Lucenti, A. Forni, C. Botta, L. Carlucci, C. Giannini, D. Marinotto, A. Previtali, S. Righetto and E. Cariati, *J. Phys. Chem. Lett.*, 2017, **8**, 1894-1898.

ARTICLE

Journal Name

- 61 E. Lucenti, A. Forni, C. Botta, L. Carlucci, C. Giannini, D. Marinotto, A. Pavanello, A. Previtali, S. Righetto and E. Cariati, *Angew. Chem. Int. Ed.*, 2017, **56**, 16302-16307.
- 62 G.-P. Yong, Y.-M. Zhang, W.-L. She and Y.-Z. Li, *J. Mater. Chem.*, 2011, **21**, 18520.
- 63 Y. Gong, L. Zhao, Q. Peng, D. Fan, W. Z. Yuan, Y. Zhang and B. Z. Tang, *Chem. Sci.*, 2015, **6**, 4438-4444.
- 64 S. Kuno, H. Akeno, H. Ohtani and H. Yuasa, *PCCP*, 2015, **17**, 15989-15995.
- 65 Z. Cheng, H. Shi, H. Ma, L. Bian, Q. Wu, L. Gu, S. Cai, X. Wang, W.-w. Xiong, Z. An and W. Huang, *Angew. Chem. Int. Ed.*, 2018, **57**, 678-682.
- 66 S. Kuno, T. Kanamori, Z. Yijing, H. Ohtani and H. Yuasa, *ChemPhotoChem*, 2017, **1**, 102-106.
- 67 Z. Chai, C. Wang, J. Wang, F. Liu, Y. Xie, Y.-Z. Zhang, J.-R. Li, Q. Li and Z. Li, *Chem. Sci.*, 2017, **8**, 8336-8344.
- 68 J. Yang, Z. Ren, Z. Xie, Y. Liu, C. Wang, Y. Xie, Q. Peng, B. Xu, W. Tian, F. Zhang, Z. Chi, Q. Li and Z. Li, *Angew. Chem. Int. Ed.*, 2017, **56**, 880-884.
- 69 A. Mukherjee, S. Tothadi and G. R. Desiraju, *Acc. Chem. Res.*, 2014, **47**, 2514-2524.
- 70 S. Cai, H. Shi, D. Tian, H. Ma, Z. Cheng, Q. Wu, M. Gu, L. Huang, Z. An, Q. Peng and W. Huang, *Adv. Funct. Mater.*, 2018, 1705045.



Organic materials showing solid state RTP induced by XB and/or π - π intermolecular interactions among one-type only molecules are reviewed.